香港氣象學會

HONG KONG METEOROLOGICAL SOCIETY

Bulletin

VOLUME 10, NUMBER 1/2, 2000

ISSN: 1024-4468

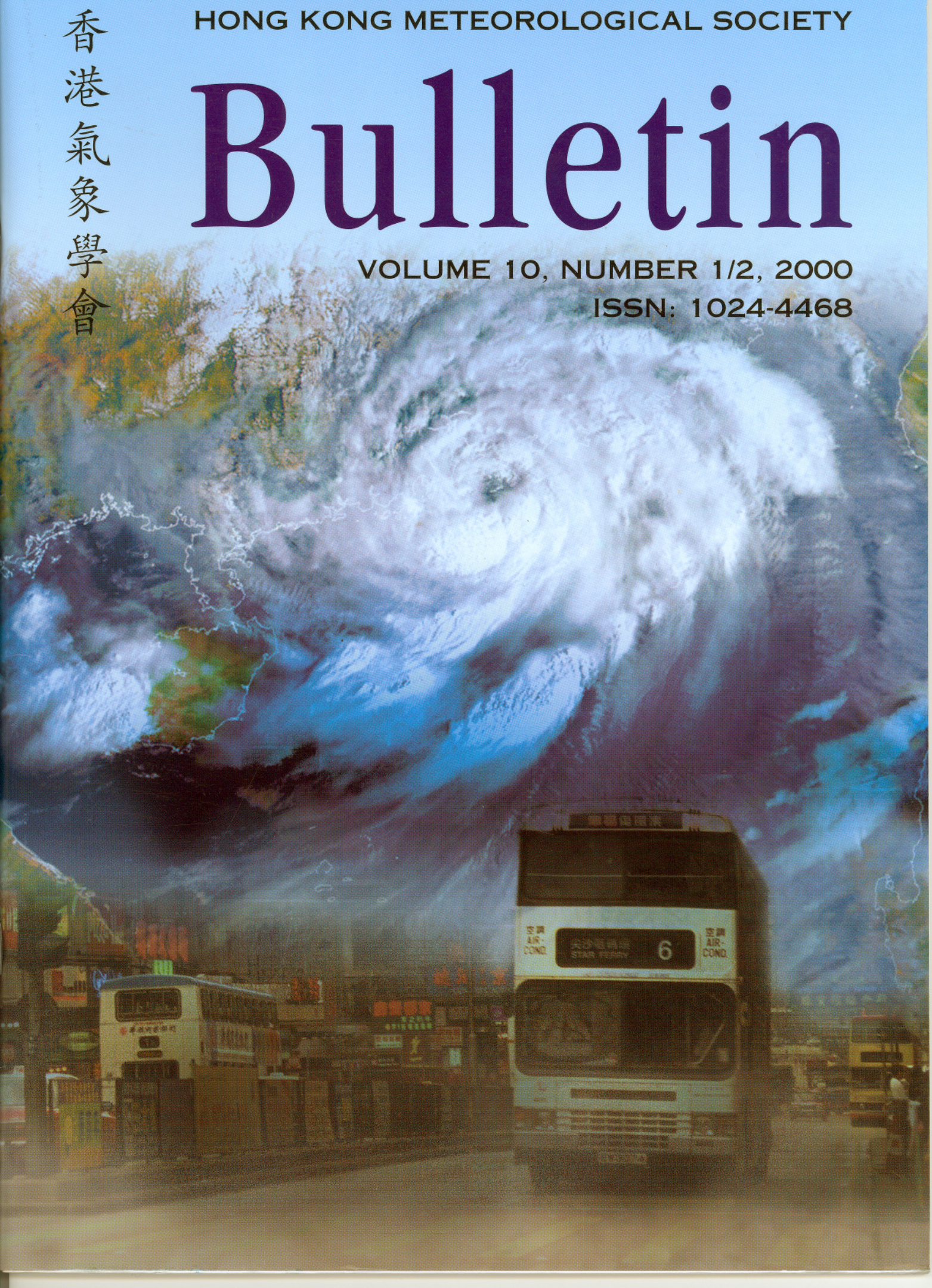

ISSN 1024-4468

The Hong Kong Meteorological Society Bulletin is the official organ of the Society, devoted to articles, editorials, news and views, activities and announcements of the Society.

Members are encouraged to send any articles, media items or information for publication in the Bulletin. For guidance see the "information for contributors" in the inside back cover.

Advertisements for products and/or services of interest to members of the Society are accepted for publication in the BULLETIN.

For information on formats and rates please contact the Society secretary at the address opposite.

Views and opinions expressed in the articles or any correspondence are those of the author(s) alone and do not necessarily represent the views and opinions of the Society.

The mention of specific products and/or companies does not imply there is any endorsement by the Society or its office bearers in preference to others which are not so mentioned.

SUBSCRIPTION RATES (Two issues per volume)

Institutional rate:	HK$ 300 per volume
Individual rate:	HK$ 150 per volume

Published by

The Hong Kong Meteorological Society

c/o Hong Kong Observatory
134A Nathan Road
Kowloon, Hong Kong

香港氣象學會

HONG KONG METEOROLOGICAL SOCIETY

Bulletin

Volume 10, Numbers 1/2, 2000

CONTENTS

Editorial

This issue of the Bulletin combines two issues in one volume and contains three papers.

The first paper by Mickey Man-Kui Wai of Plum Rain Solutions, Tallahassee, Florida, USA, uses surface synoptic analyses and radiosonde data of the Hong Kong Observatory along with hourly measurements from air quality monitoring stations of the Hong Kong Environmental Protection Department, to re-examine the development of two air pollution events previously examined by Chen, Kot and Tepper (1996) in ***HKMetS Bulletin Vol. 6, No.1.*** He concludes that the observations do not support the view expressed in that paper on the suitability of a radio acoustic sounding system (RASS) as a supplemental air quality detection system in Hong Kong.

In the second paper, also by Mickey Wai, climatological typhoon track data are examined to provide useful insights into the characteristics of typhoons affecting Hong Kong, in particular in relation to typhoon intensity in the South China Sea. This paper forms Part 1 of a series to appear in forthcoming issues of the ***Bulletin.***

The third paper by Mervyn R. Peart and Bill Kyle of the Department of Geography and R.D. Hill of the Department of Ecology and Biodiversity, The University of Hong Kong provides a preliminary report on efforts to test the feasibility of extracting water from clouds passing over upland areas in Hong Kong in order to gain some insight into the factors relevant to the process. The paper describes the design and construction of an instrument, termed a neblinometro, which was exposed near the summit of Tai Mo Shan, and reports on preliminary results obtained from the instrument.

The Editorial Board, as always, look forward to receiving any opinions, suggestions or contributions sent in by readers.

Bill Kyle, Editor-in-Chief

Mickey M.K. Wai

Plum Rain Solutions, 2019 Skyland Drive, Tallahassee, FL 32303, USA

On the Development of Two Cases Of Air Pollution in Hong Kong

Abstract

The surface synoptic analyses and the radiosondes of the Hong Kong Observatory and the hourly measurements of the Hong Kong Environmental Protection Department air quality monitoring stations are used to re-examine the development of two air pollution events. The observations do not support the conclusions made by Chen *et al.* (1996) in a recent study on the suitability of a radio acoustic sounding system (RASS) as a supplemental air quality detection system in Hong Kong. This note stresses that the surface synoptic analyses, routine radiosondes, and the hourly measurements of air quality monitoring stations over the territory are invaluable in air pollution forecasting.

Introduction

Recently, Chen *et al.* (1996) proposed that a radio acoustic sounding system (RASS) at a site within the campus of Hong Kong University for Science and Technology (HKUST) in Clear Water Bay is suitable for a supplemental air quality detection system in Hong Kong. Using a series of RASS temperature soundings over a period of 3 to 5 hours from two synoptic weather systems, Chen *et al.* (1996) concluded that the RASS enabled air quality forecasters to monitor the evolution and dissipation of the inversion, which might fumigate the pollutants to the surface layer. However, the results presented in the article did not substantiate such a conclusion. In both cases, no evidence indicated that air pollutants were fumigated into the surface layer. Furthermore, in their discussion, Chen *et al.* (1996) stated that "On January 3, 1996 a distinctly less stable atmosphere CURIOUSLY raised the air pollution index (API) to a record breaking 120". Chen *et al.* (1996) seem to admit that they do not know what circumstance would make such a situation of high API. Therefore, there are four objectives of this note. The first objective is to examine the predictability of RASS in air pollution forecast. The second objective gives some insights into what meteorological situations would lead to the severe air pollution events. The third objective provides a general view of temporal and spatial distributions of air pollutants over the territory using the air quality measurements of Hong Kong Environmental Protection Department (HKEPD). Finally, the fourth objective is to stress the importance of Hong Kong Observatory (HKO) surface synoptic analyses and soundings in air pollution forecasts.

Data

This study is based on two data sets. The first data set is the seven launches of radiosondes of the Hong Kong Observatory, which are summarized in Table 1. Furthermore, these meteorological elements are used to

Table 1. Summary of the radiosonde data. Hong Kong local time (HKT) is used.

Time	Date	Meteorological Elements
2000	December 17,1995 January 2, 1996 January 3, 1996	Geopotential height, pressure, air temperature, dew point, relative humidity, and wind velocity
0800	December 18, 1995 January 3, 1996	geopotential height, pressure, air temperature, dew point, relative humidity, and wind velocity
1400	December 18, 1995 January 3, 1996	geopotential height, pressure, and wind velocity

calculate the specific humidity, dew-point depression, and virtual potential temperature (θ_v), and static stability. In particular, both relative humidity and dew-point depression are used to locate the inversion layer and the cloud layer. The static stability ($\Gamma_{\theta v}$) in the boundary layer is defined as follows: stable if $\Delta\theta_v/\Delta z > 0$, well-mixed or uniform if $\Delta\theta_v/\Delta z > 0$, and unstable if $\Delta\theta_v/\Delta z < 0$. The vertical lapse rate, Γ, is calculated from the RASS temperature.

The second data set is the hourly air quality measurements at the nine Hong Kong Environmental Protection Department (HKEPD) stations for the month of January in 1996. A brief summary of these stations and their environments is shown in Table 2. Among these stations, Tsuen Wan, Kwai Chung, Sham Shui Po, Mong Kok, Central-Western, and Kwun Tong are urban stations; Mong Kok is a roadside station; Yuen Long, Tai Po, and Shatin are new town stations. Hourly measurements at these stations include NO_x, SO_2, air temperature, wind velocity, ozone, CO, and suspended particulates. The instruments are mounted at the altitudes ranging from 17 m to 25 m above the ground.

Table 2. Locations of Nine Air Quality Monitoring Stations

Name of Station	Height	Environment
Central-Western	18 m	Urban
Kwai Chung	25 m	Urban
Kwun Tong	25 m	Urban
Sham Shui Po	17 m	Urban
Tsuen Wan	17 m	New Town
Shatin	21 m	New Town
Tai Po	25 m	New Town
Yuen Long	25 m	New Town
Mongkok	<5 m	Urban Roadside

In this study, measurements of NO_x and SO_2 are primarily used to provide a general view of spatial and daily distributions of air pollutants over the territory. Similarly, the hourly measurements of wind velocity are used to illustrate the surface flow patterns during the air pollution event. At stations Yuen Long and Sham Shui Po, no measurements of wind velocity are available. Note that the measurements at the Central-Western stations are not shown but they are used for discussion only.

Case 1: A Clear Day on January 3, 1996

To facilitate the discussion, the air pollution event is divided into three stages. The developing stage (Stage I) is represented by a period between 2000 HKT on January 2 and 0600 HKT on January 3, 1996. The mature stage (Stage II) is between 0700 to 0900 HKT on January 3, 1996, and the receding stage (Stage III) begins at 1000 HKT on the same day, at which time the concentration of air pollutants begins to drop continuously.

a. Patterns of Synoptic Pressure

On this day, the center of a vast surface high pressure system is located near 30°N and 110°E. Contrary to the tight pressure gradients over the interior of western China, the pressure gradients in the regions of Eastern and South China were weak. Therefore, the weak surface pressure gradient force over the South China coastal areas would produce a relatively weak surface wind speed. Assuming an inviscid flow, one can approximate the surface wind centered over Hong Kong with the geostrophic wind, $V_g = \Delta p/\rho f d$. Here, Δp is the pressure difference between two adjacent isobars, ρ is the density of air, f is the Coriolis parameter, and d is the distance perpendicular to the isobars where the pressure difference is taken. If we use Δp = 4 hPa, ρ = 1.275 kg m^{-3}, f = 5.534 * 10^{-5} s^{-1}, and d = 832 km, we obtain the geostrophic wind equal to 7 m s^{-1}, which agrees well with the boundary layer wind of 5-6 m s^{-1} as indicated by HKO on January 3, 1996.

b. Boundary Layer Structure

An antecedent, shallow boundary layer of 300 m (symbol x) occurred at 2000 HKT on January 2, 1996 (Figure 1). In the shallow boundary layer, $\Gamma_{\theta v}$ was roughly 0.0036 K m^{-1}. At 0800 HKT on January 3, 1996, nocturnal radiative cooling during the previous night had led to the formation of a very stable surface boundary layer below 560 m (symbol m) with $\Gamma_{\theta v}$ = 0.012 K m^{-1}. The stratification was about 300 percent stronger than the boundary layer at 2000 HKT in the previous evening. Throughout the night and the morning hours, the boundary layer wind came out between the northwestern and northeastern quadrant with a strong northerly component of the wind. Therefore, the mountain chains on the Hong Kong mainland sheltered most of the Hong Kong urban areas from the northerly wind. Above 560 m the air temperatures differed little after 2000 HKT on January 2, 1996. As time progressed from 0800 to 2000 HKT, the boundary layer wind began to shift from northeasterly to more easterly. Also solar heating at the ground surface transferred the stable boundary layer to a relatively well-mixed boundary layer. The mixed layer continued to grow and finally reached about 900 m by 2000 HKT (symbol c). The $\Gamma_{\theta v}$ in the boundary layer was about 0.0014 K m^{-1}.

c. Surface Winds

Although the wind records in this study are based on nine air quality monitoring stations and the radiosondes, an additional view of surface wind pattern over the territory can be filled in with the numerical results of the boundary layer winds under a light northerly flow (Yeung *et al.*, 1991), in which the synoptic situations were similar to those on January 3, 1996. The only difference is that the numerical study was carried out under a neutral condition.

Above the boundary layer, the wind over the territory was relatively simple during the entire air pollution event. At the beginning of Stage I, the synoptic wind was northwesterly. It then veered towards northeasterly and finally more easterly towards Stage III. The surface wind patterns over the territory were complicated (Figure 2), indicative of the effects of the local topography and surface heating and cooling.

Figure 1. Vertical profiles of virtual potential temperature at three consecutive times: letter x represents 2000 HKT on January 2, 1996; letter m represents 0800 HKT on January 3, 1996, and letter c represents 2000 HKT on January 3, 1996.

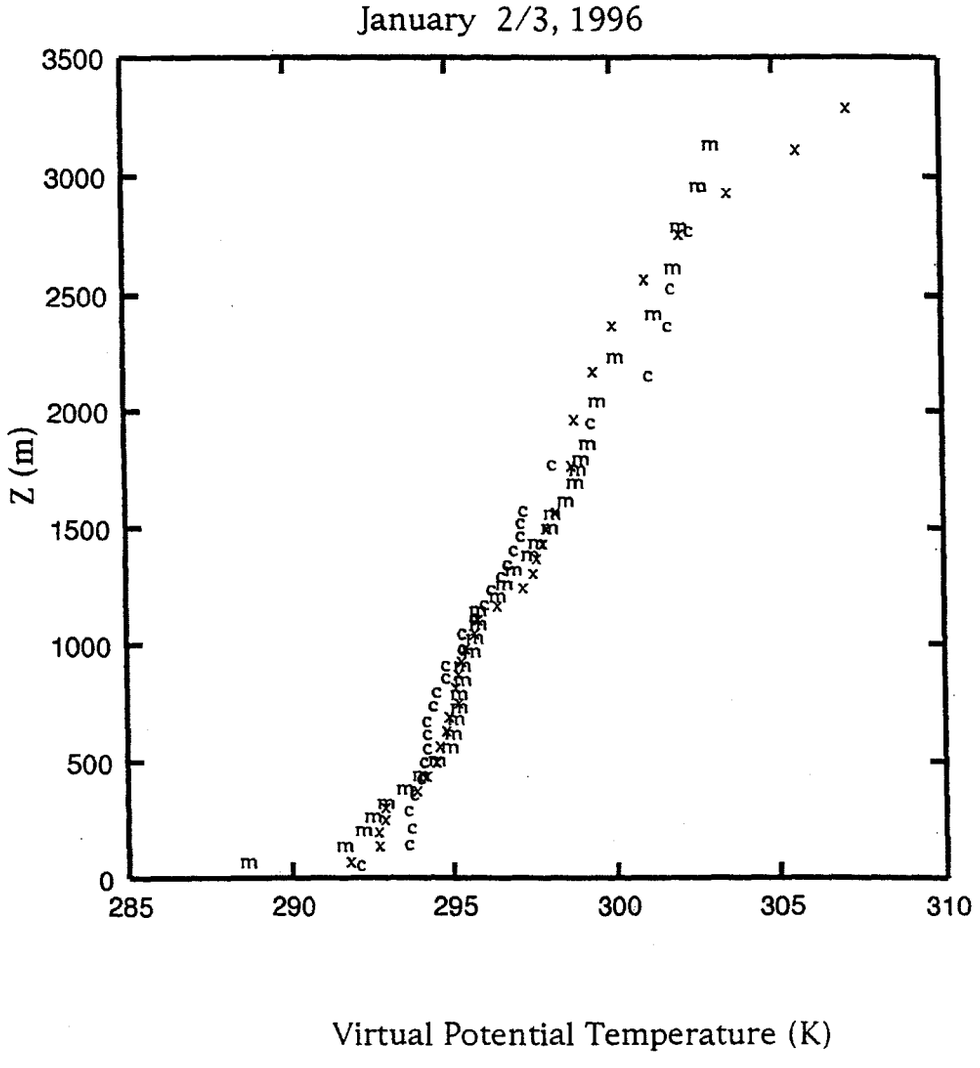

During Stage I, the surface wind was northwesterly over a relatively flat terrain in the upwind region of the major northeastern-southwestern mountain chain (Tai Mo Shan on the Kowloon Peninsula to Sunset Peak and Lantau Peak on Lantau Island).

In the eastern New Territories, the surface wind backed towards more westerly as it was forced through the gap between Pat Sin Leng and Tai Mo Shan, as indicated by the surface wind at the Tai Po station. By noon on January 3, 1996, the surface wind changed to southeasterly as the synoptic wind changed to more easterly. Over Shatin, the surface wind acted like a mountain-valley wind system: mountain wind (southwesterly) in Stage I and valley wind (northeasterly) in Stage III.

Figure 2. The time series of the surface wind velocity at six air quality monitoring stations. The wind directions are given by solid lines and the wind speeds are given by the magnitude of the histograms.

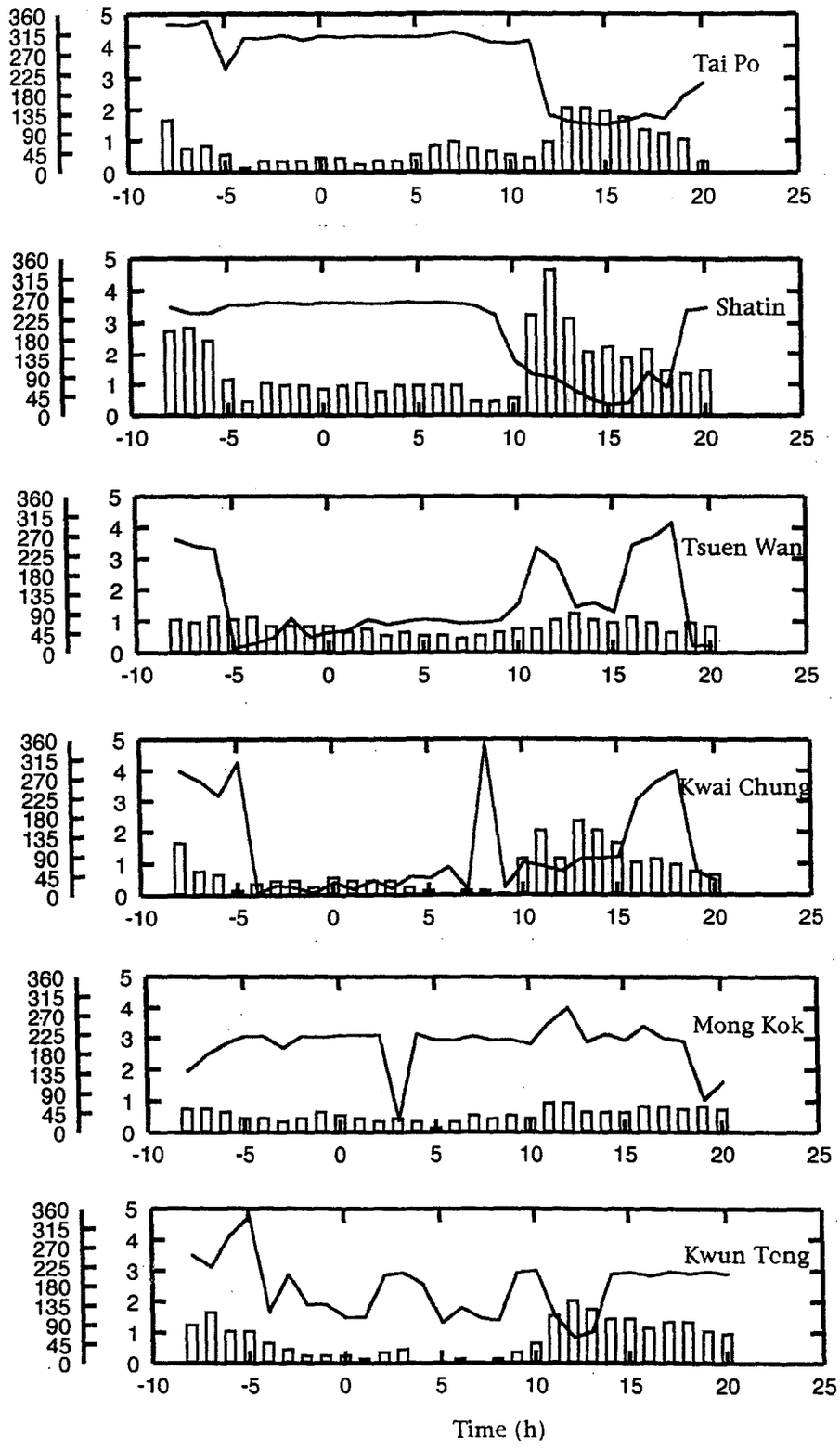

In the western New Territories, the surface flow split into two branches as the northerly flow approached Lantau Island. One branch entered the harbour through the corridor over Kap Shui Mun with a strong westerly component of the wind (*i.e.* a strong westerly component of the surface wind at the Central-Western station on the water front of Hong Kong Island). As the synoptic winds shifted to a more easterly in Stages II and III, the surface wind in the harbour also showed a strong easterly component of the synoptic wind.

On the lee side of Tai Mo Shan, the surface winds over Tsuen Wan and Kwai Chung were quite similar. In Stage I, the surface winds had a strong northerly component and then southeasterly in Stage III. Further east over the Kowloon Peninsula, the prevailing surface wind came from the western direction. Over Kwun Tong, the surface wind was quite variable in Stages I and II

Although the surface flow pattern was complex over the territory, the winds over were relatively calm (less than 1 m s^{-1}) during most of Stage I and Stage II. Around 1100 HKT, the surface wind speed over the territory began to increase. However, in the inner city areas such as Mong Kok, the surface wind remained relatively calm.

In short, a weak surface pressure gradient force of a surface high pressure system over the South China coastal area brought relatively weak northerly synoptic winds to the Hong Kong territory. The mountain chains sheltered most of the urban areas from the northerly wind and produced a calm condition. Associated with the weak synoptic wind was large-scale subsidence, which prohibited convection and subsequently the growth of the boundary layer. Furthermore, nocturnal radiative cooling at the surface led to the formation of a low level stable boundary layer, which would trap pollutants close to the surface. Under the calm wind condition, the horizontal dispersal of air pollutants would also be minimal.

d. Diurnal and Spatial Distributions of SO_2 and NO_x

Superimposed on the topographical map of Hong Kong are the time series of hourly concentrations of SO_2 and NO_x in mg m^{-3} at eight air quality stations starting from 1600 HKT on January 2, 1996 to 2000 HKT on January 3, 1996. The 12-hour measurements of SO_2 and NO_x prior to and after the severe air pollution event near 0900 HKT on January 3, 1996 are also included for the purpose of seeking evidence of downwind transport of air pollutants. Furthermore, a longer time series of the concentration of air pollutants would also help to estimate the length of time required for the event to subside.

In Figure 3, the stations are arranged from north to south and from west to east. In the top row are Yuen Long, Tai Po, and Shatin, which are located north of the major mountain chains. The stations in the middle row are Tsuen Wan and Kwai Chung, which are located in the western part of New Kowloon. The stations in the bottom row are Sham Shui Po, Mongkok, and Kwun Tong; all of which are in the urban area. The concentrations of NO_x (blank) and SO_2 (black) are represented by the magnitude of histograms.

Nine stations showed bimodal concentrations of SO_2 and NO_x. The first maximum occurred near 0900 HKT on January 3, 1996. Note that the concentrations of SO_2 and NO_x peaked near 1000 HKT at Mong Kok roadside station. The second maximum occurred in the late evening on January 2, 1996. In the New Towns, the duration of high concentration of NO_x was shorter and the maximum concentration of NO_x peaked around 2000 HKT. However, in the inner urban areas (Mongkok), the duration of high concentration of NO_x was longer and the maximum concentration of NO_x peaked near midnight.

In order to determine if the occurrence of the bimodal distribution was an isolated incidence, two daily cycles of hourly mean concentrations of NO_x and SO_2 were calculated based on the 31 days (C31) and 29 days (C29) records. The 29-day mean daily cycle excluded the records on January 2 and 3. The daily cycles of C31 and C29 also showed bimodal maxima of NO_x and SO_2 in the late evening near 0900 HKT. Therefore, the timing of occurrence of the bimodal distributions of pollutant was of a climatological nature.

Figure 3. The hourly measurements of NO_x (blank histogram) and SO_2 (dark histogram) in mg m^{-3} at eight air quality monitoring stations (open circles) in Hong Kong. Yuen Long, Tai Po, and Shatin are New Town stations. Tsuen Wan, Kwai Chung, Sham Shui Po, and Kwun Tong are urban stations. Mongkok is an urban road side station.

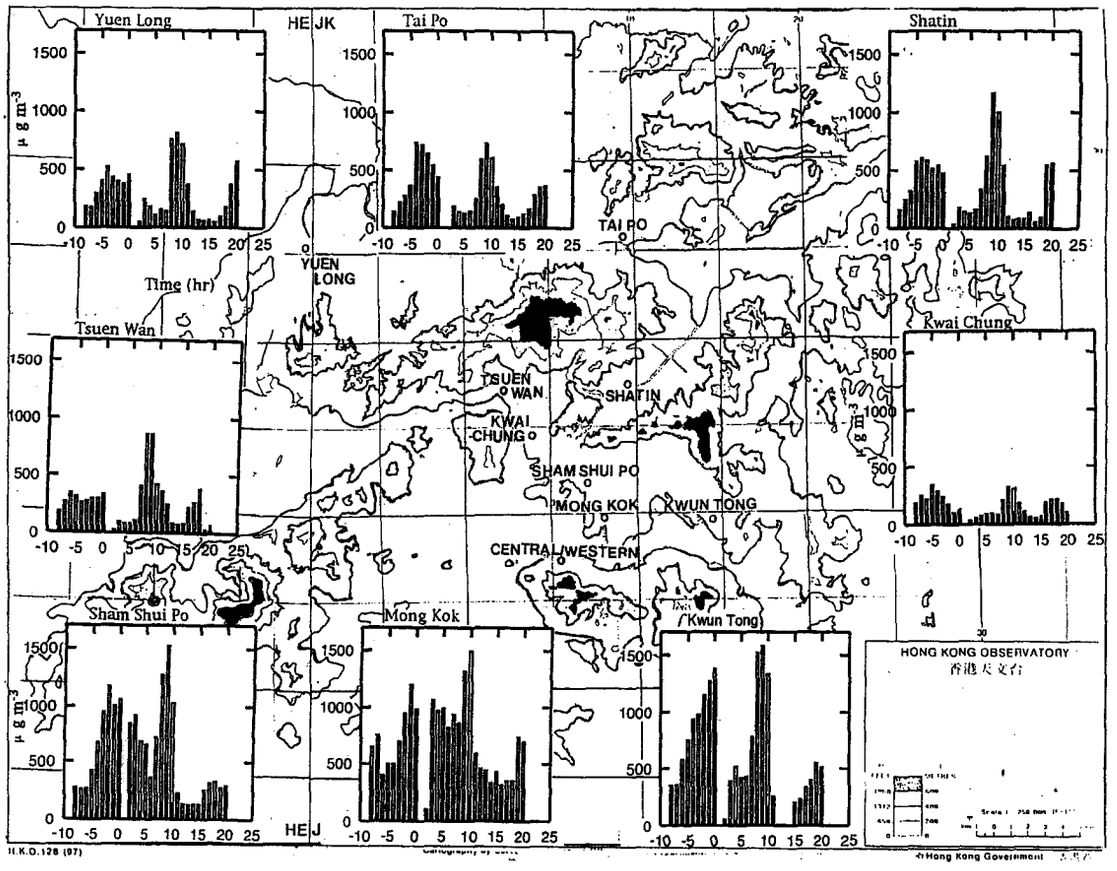

While the timing of the peak concentration remained relatively unchanged, the peak concentration of C29 was about 20-25 percent smaller than those of C31. Consequently, a daily occurrence of the air pollution event shortly after dawn can readily develop into a severe air pollution event with record breaking concentrations of air pollutants if favorable meteorological conditions are present.

There is no evidence supporting the view that air pollutants are fumigated into the surface layer. The rapid increase in the concentration of NO_x actually occurs between 0700 and 0800 HKT at Kwai Chung, Kwun Tong, Sham Shui Po, Tsuen Wan, Tai Po, and Yuen Long (Table 3) when the stratification is the strongest near the surface. Note that the stratification ($\Gamma_{\theta v}$) below 136 m is equal to 0.024 K m^{-1} even though the top of the stable boundary layer is located near 560 m (Figure 3). Between 0800 and 0900 HKT, the rate of increase in the concentration of NO_x at these stations is slower even though the solar heating at the surface changes the stable boundary layer to a relatively well-mixed boundary layer.

As shown in Figure 3, the relatively bigger increase of NO_x occurs between 0800 and 0900 HKT at the Mongkok roadside station and Shatin station. The delay at these two stations is probably because the rush hour does not end till 0900 HKT. From 1000 HKT onwards, the concentrations of NO_x begin to drop at every station, as the mixed layer grows deeper. Moreover, the concentrations of NO_x and SO_2 plunge beginning from 1100 HKT as the surface easterly wind begins to increase. Therefore, fumigation of air pollutants does not occur over the territory because most of the rapid increase of air pollutants at the surface occurs under a stable boundary layer condition.

Table 3. Time rates of change of the NO_x (mg m^{-3} h^{-1}) at the air quality monitoring stations. $D(NO_x)1$ refers to the changes of NO_x between 0700 and 0800 HKT. Similarly, $D(NO_x)2$ refers to the changes of NO_x between 0800 and 0900 HKT.

Name of Station	Height	$D(NO_x)1$	$D(NO_x)2$
Kwai Chung	25 m	133	117
Kwun Tong	25 m	739	62
Sham Shui Po	17 m	554	253
Tsuen Wan	17 m	456	-8
Shatin	21 m	289	540
Tai Po	25 m	346	136
Yuen Long	25 m	614	55
Mongkok(Roadside)	<5 m	-74	451

No direct evidence suggests that the downwind transport of foreign pollutants leads to the occurrence of the severe air pollution on January 3, 1996. First, the synoptic wind system over the territory is weak and dominated by the local wind systems. Second, the maximum concentration of air pollutants at nine stations occurs almost simultaneously. There is no time lag of peak concentrations of the NO_x and SO_2 between the upwind station and the downwind stations. For instance, the location of the industrial complexes in the Shenzhen Special Economical Zone north of the Hong Kong border is mostly located near Deep Bay (Hsu, 1983). The northerly flow would advect the pollutants to the open sea. If the downwind transport of pollutants occurs, the maximum concentration of NO_x at Tusen Wan and Kwun Tong would lag 3-4 hours and 5-6 hours behind Sha Lo Wan (on Lantau Island) respectively.

In summary, the synoptic situations on January 2-3, 1996 brought a calm condition along with large-scale subsidence to the Hong Kong areas. The depth of the boundary layer at 2000 HKT was below 400 m on January 2, 1996. An elevated inversion was capped at 1100 m. The boundary layer wind primarily came out of the north. Throughout the night, the nocturnal radiative cooling at the ground surface led to the formation of a stable boundary layer. At 0800 HKT on January 3, 1996, the top of stable boundary layer was located near 560 m. The strongest stratification was found below 136 m. The fastest increase of emissive NO_x and SO_2 at the surface occurred between 0700 and 0800 HKT when the lower boundary layer was the most stable. Under the calm wind condition, the horizontal dispersal of pollutants was minimal. Therefore, the accumulation of emissive pollutants increased at the surface. As the solar heating at the surface began, the stable boundary layer at the surface was changed into a relatively well-mixed boundary layer. The surface air pollutants were transported upward and beginning to decrease at the surface. Around noon, the boundary layer wind shifted to a more easterly coupled with stronger surface winds over the territory. The concentration of pollutants in the boundary layer dropped drastically. As time progressed, the mixed layer continued to grow to about 900 m by 2000 HKT.

e. The RASS temperature profiles

When comparing the RASS temperature profiles and from what we know about the boundary layer structure on January 3, 1996, one can find the deficiencies in RASS and several disagreements. First, Chen *et al.* (1996) have stated that the vertical extent of the RASS goes up to 1 km. Yet in their Figures 2 and 3, all the RASS temperature profiles are omitted near the ground surface and in the upper level beneath 1 km, especially for those between 0800 and 1100 HKT on January 3, 1996.

The omission of the sounding below 200 m level can be easily understood by the fact that the RASS is located at the top of a building. The setup is a deficiency because it generally misses the nocturnal stable boundary layer, the depth of which is of the order of 10 m. The nocturnal stable boundary layer height is an important parameter in the practical models forecasting the dispersal of pollutants during winter months (Hunt, 1981). As concluded by HKEPD, the traffic emissions remain one of main local sources of air pollution in Hong Kong (Planning Department, 1996). The omission of the boundary layer top in the RASS profiles, whether they are resulted from either the limitation of RASS under certain meteorological phenomenon or man-made, neglects an important parameter in the practical models for convective plumes (Lamb, 1981). Since the boundary layer frequently contains multiple layers of different lapse rate (Nai-Ling *et al.*, 1983; Koo *et al.*, 1984; Wai *et al.*, 1997), it is a poor predictor in air pollution forecasts when using $\Gamma_{\theta v}$ or Γ alone. It becomes less objective as to what thickness and at what height this lapse rate should be determined. Furthermore, there are large differences in the lapse rate depending on the heights chosen. For instance, at 0900 HKT, the Γ for a deeper boundary layer between 150 and 450 m is 0.0053 K m^{-1}. However, if the layer is taken between 150 and 260 m, the Γ is 0.0090 K m-1. Similarly, the Γ in an elevated layer between 260 and 400 m is about 0.0014 K m^{-1}. Therefore, the boundary layer is relatively well mixed below 300 m while it is relatively stable aloft.

Chen *et al.* (1996) need to confirm that the RASS inversion at 1000 HKT (less than 1°C) is indeed located between 400 and 450 m (represented by two data points). The justification in correlating the API at Sha Lo Wan (on Lantau Island) to the Γ at HKUST (in Clear Water Bay) is required because they are about 30 km apart. Furthermore, the record breaking API at Sha Lo Wan around 1000 HKT does not corroborate with the maximum concentrations of NO_x and SO_2 at most of the stations in Hong Kong (Figure 3).

At 1130 HKT, the RASS temperature profile shows a relatively well-mixed boundary layer below 500 m. Therefore, a Γ of 0.009 K m^{-1} does not necessarily refer to the breakup of the inversion at this hour. It only means that the RASS captures a snap shot of a relatively well-mixed boundary layer. We recall that the top of the stable boundary is located near 560 m at 0800 HKT. Instead of interpreting that the breakup of the inversion occurs at 1130 HKT, it is more correct to indicate that the boundary layer top (the base of inversion) has grown deeper, or the RASS misses the top of the boundary layer.

f. Growth of the Boundary Layer

On January 3, 1996, local winds and solar heating at the ground surface were important mechanisms in the dispersal of air pollutants. Wai *et al.* (1995) analytically examined various aspects of local circulation and wind systems over Hong Kong in detail. The growth of the boundary layer is briefly described here. One can derive the prognostic equation for the top of boundary layer (or the base of the inversion) as

$$\partial Z/\partial t = -U_j \ \partial Z/\partial x_j + W_e + W_L \qquad (1)$$

Where t is time, $-U_j \ \partial Z/\partial x_j$ is the horizontal advection of the inversion base. The entrainment rate at the inversion base, W_e, is given by

$$W_e = -a \, w' \theta' / \Delta\theta \qquad (2)$$

where coefficient a ranges from 0.1 to 0.3, $\Delta\theta$ is the temperature difference across the entrainment zone at the top of the mixed layer, and $w'\theta'$ is the surface turbulent heat flux which is directly proportional to the solar heating at the ground surface. In general, the surface sensible heat flex can be calculated from the similarity relations. The large-scale subsidence, W_L, is expressed as

$$W_L(Z) = -f \, D(z)dz \qquad (3)$$

forecasting products. If the divergence can be assumed constant with height, then

$$W_L(Z) = - D \bullet Z \qquad (4)$$

If we assume the horizontal advection of inversion is zero (*i.e.* quasi-steady synoptic situation with little vertical wind shear), we can obtain an equation for Z after we substitute W_e and W_L into Equation 1. After rearranging, we obtain

$$dZ/(W_e - DZ) = dt \qquad (5)$$

The solution to Equation 5 is

$$Z(t) = W_e/D - [\, W_e/D - Z(t_o) \,]\, e^{-D(t-to)} \qquad (6)$$

If the horizontal advection of the inversion is small, the growth of the boundary layer is directly proportional to the surface heating and inversely to the large-scale subsidence. Figure 4 presents three cases of the growth of a boundary layer with three sets of W_e and W_L. The symbol square indicates that the boundary layer top reaches about 300 m at 2000 HKT with W_e = 0.02 m s^{-1} and D = 6 * 10^{-5} s^{-1}. If W_e is increased to 0.1 m s^{-1} while D is kept at 6 * 10^{-5} s^{-1}, the boundary layer will grow deeper to 1500 m at 2000 HKT (symbol diamond). Therefore, a stronger surface heating results a deeper boundary layer height if the surface divergence is kept constant. The boundary layer, marked by symbol circle, grows to 850 m at 2000 HKT with W_e = 0.07 m s^{-1} and D = 8 * 10^{-5} s^{-1} and agrees well with the observed boundary layer height (900 m).

Figure 4. **The growth of boundary layer under three sets of large-scale subsidence (W_L) and entrainment rate (W_e). Symbol diamond : D = 6 * 10^{-5} s^{-1} and W_e = 0.1 m s^{-1}. Symbol circle : D = 8 * 10^{-5} s^{-1} and We = 0.07 m s^{-1}. Symbol square : D = 6 * 10^{-5} s^{-1} and We = 0.02 m s^{-1}. Here D is the surface divergence.**

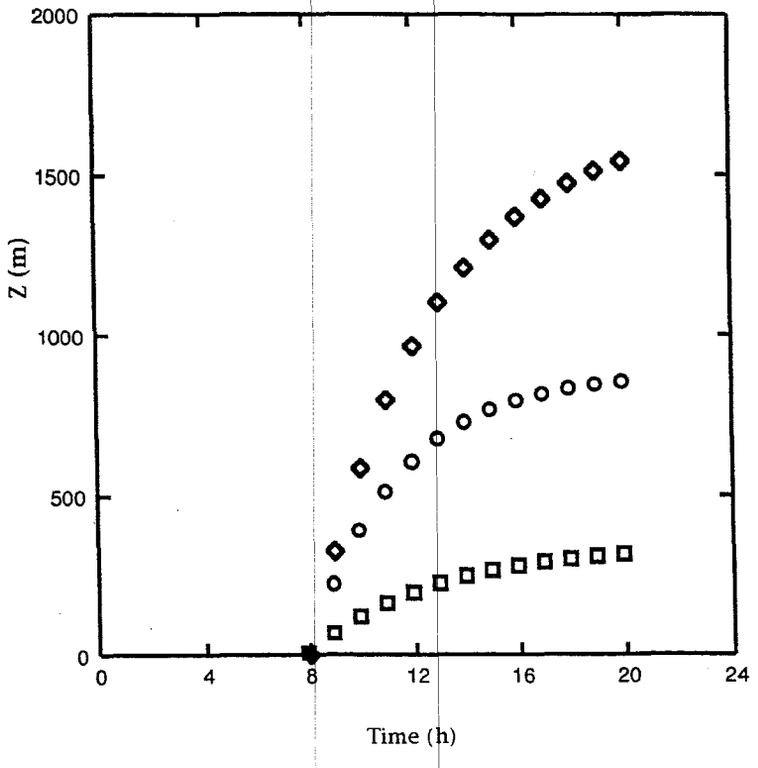

Case 2 : A Cloudy Day on December 18, 1995

a. Patterns of Synoptic Pressure and Synoptic Wind

A cold front approaching the South China coastal areas marked the synoptic situation on this day. The surface isobars were concentrated near 25°N. Note that the isobars over the oceanic area south of Hong Kong were not tight probably because of a lack of oceanic observations. Ahead of the cold front was a broad region of large-scale vertical advection (of an order of a few cm s^{-1}), which transported pollutants upwards. If the ascending moist air parcels resulted in clouds and precipitation, precipitation scavenging would remove pollutants from the atmosphere. Additionally, a strong pressure gradient force over the South China coastal areas would produce a region of stronger wind. If we repeat the calculation as described in Case 1, we obtain the geostrophic wind equal to 15 m s^{-1} with ΔP = 6 hPa and d = 556 km. The estimation is comparable to the observed boundary layer wind of 10 m s^{-1} on December 17, 1995.

b. Boundary Layer Structure

The relative humidity sounding at 2000 HKT on December 17, 1995 already showed a deep, solid cloud layer between 450 m and 2250 m (Figure 5). The boundary layer at this time was in the warm sector of the surface front. By 0800 HKT on December 18, 1995, the cold front had penetrated the territory because of the cooler temperature (symbol y) and lower specific humidity (symbol o) in the boundary layer. Behind the cold front, the cloud layer was less solid vertically and less homogeneous horizontally because of the appearance of two cloud layers: one between 420 and 700 m and a second between 790 m and 1140 m. Considering the characteristics of cloud distribution behind the cold front, we may conclude that the cloud layer is actually between 420 m and 1140 m. The subcloud layer was relatively well mixed ($\Gamma_{\theta v}$ = 0.0007 K m^{-1}). The $\Gamma_{\theta v}$ inside the cloud layer at 0800 HKT was 0.015 K m^{-1}.

c. RASS Temperature Profiles

By similar argument to that used for Case 1, the use of Γ alone as a predictor is a poor choice for a pollution event. Additionally, Chen *et al.* (1996) need to provide reasons for the justification to compare the Γ derived from the 0800 HKT HKO radiosonde with the Γ derived from the 0930 HKT RASS temperature profile. Is the 0800 HKT RASS temperature profile unreliable? Second, the cloud layer in this case, which also marks the inversion layer, is advected over the territory and is also beginning to dissipate. Therefore, the thickness and location of the cloud layer as well as the temperature lapse rate inside the cloud layer are undergoing rapid changes.

Discussion

In Cases 1 and 2, the HKO surface synoptic analyses and radiosondes unambiguously show two different weather systems, which dynamically control the dispersal processes of air pollutants in the boundary layer. Needless to say, both data sets are crucial to the forecasts of the air pollution events. Also, the hourly measurements from the HKEPD air quality monitoring stations have provided insight into the diurnal and spatial distributions of air pollutants over the territory. In Case 1, the synoptic situation organized large-scale subsidence and calm wind conditions over the South China coast. Furthermore, the local mountain chains sheltered most of the urban areas. Then, the local nocturnal radiative divergence throughout the night at the ground surface led to the formation of a stable boundary layer. The fastest increase of emissive NO_x and SO_2 occurred between 0700 and 0800 HKT when the surface stable boundary layer was strongest. As the solar heating heats the ground surface, the surface stable boundary layer was changed into a relatively well-mixed boundary layer. The growth of the boundary layer brought pollutants upwards and led to the reduction of pollutants at the surface. Several hours later, the increased advective process dispersed the surface pollutants in the urban areas.

Figure 5. Vertical Profiles of virtual potential temperature (letters m and y) and specific humidity (letters x and o) at two different times : letters m and x represent 2000 HKT on December 17, 1995 while letters y and o represent 0800 HKT on December 18, 1995.

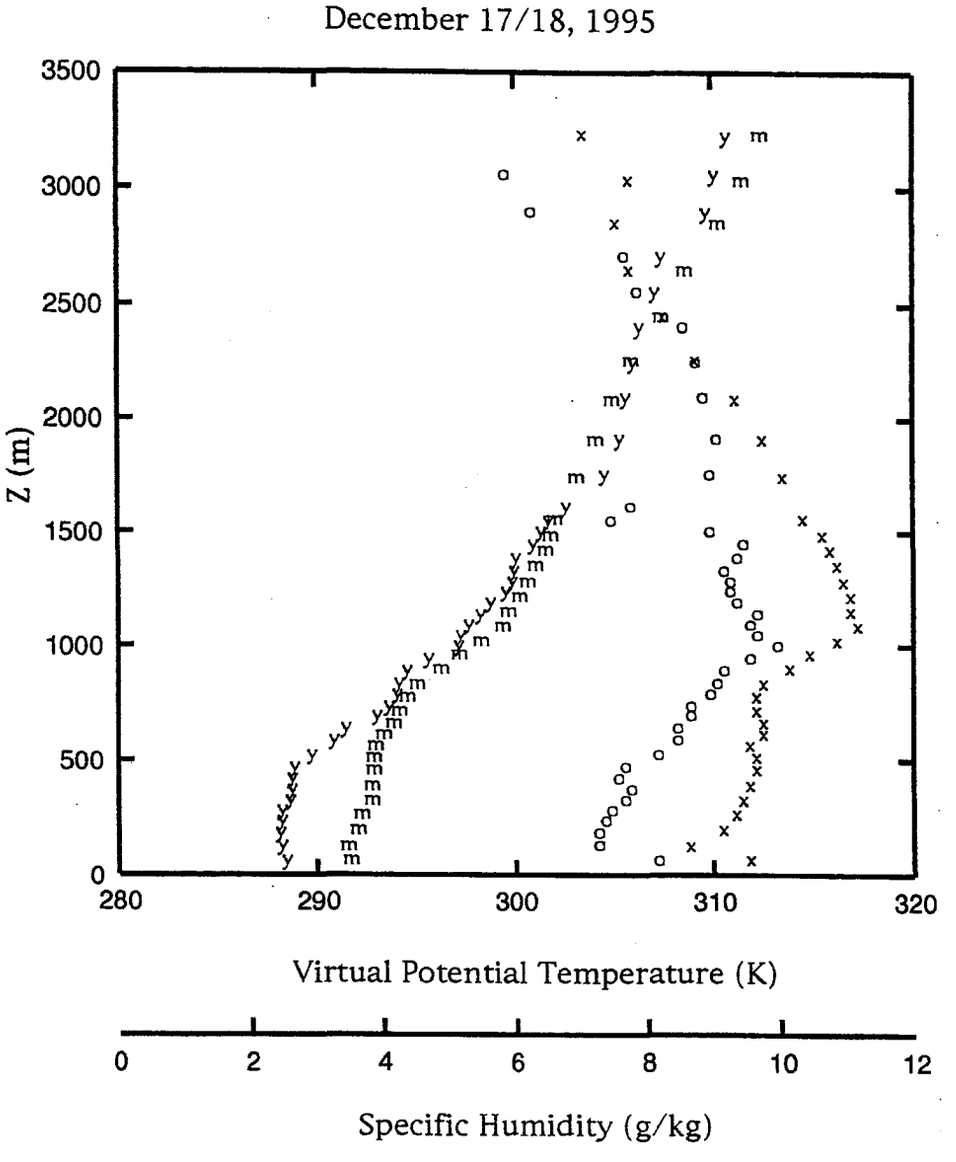

In Case 2, the synoptic situation was dominated by a frontal passage through Hong Kong. Strong wind and large-scale ascent motion, coupled with frontal precipitation, were the effective mechanisms for the removal of air pollutants in the boundary layer.

If we consider the boundary layer processes instead of the static stability, then we do not encounter ambiguous conclusions such as "On January 3, 1996 a distinctly less stable atmosphere CURIOUSLY raised the API to a record breaking 120". Therefore, the derived RASS temperature lapse rate alone as described by Chen *et al.* (1996) is a poor predictor in forecasting the air pollution events.

In air pollution forecasts, four important parameters are wind velocity, boundary layer height, surface roughness length, and atmospheric dispersion (Szepesi, 1987). Among these four parameters, wind velocity is the most important one because of its varying spatial scales: continental, regional, urban, and site-specific.

At the continental scale (~1000 km), air pollution forecasters primarily focus on the large-scale wind system, which can be derived from the location of surface high and surface low pressure systems and locations of frontal cloud bands. Depending upon the strength of synoptic wind and the position of Hong Kong relative to the emissive source, one can estimate the length of time for the pollutants to reach Hong Kong. For instance, if the synoptic wind in the boundary layer remains steady at 5 ms^{-1}, it will take 2 days before the imported pollutants affect the air quality in Hong Kong. Because of atmospheric dilution, the severity or the dosage of the pollutants may not be life threatening. However, the pollutants will add to the local concentration as background pollutants.

At the regional scale (~100 km), it will take about 5 hours for the emissive pollutants from the source to reach Hong Kong if the boundary layer wind is 5 m s^{-1}. Similar to the continental scale, the regional wind system, large-scale vertical motion, and frontal cloud system are still important factors in air pollution forecasts because the synoptic weather system will set the stage as to how the air pollutants are transported. Therefore, depending on the nature of the regional scale pollutants, this background pollutant can modify the diurnal concentration of local pollutants. Additionally, forecasters need to understand how the meso-scale wind system interacts with the synoptic wind system and when the meso-scale wind system becomes dominant.

At the urban scale (~10 km) air pollution forecast, the boundary layer wind of 5 m s^{-1} will carry pollutants from the emissive source to a downwind community in 30 minutes. Therefore, the source of pollutants is local in nature, and there are two considerations in forecasting air pollution events.

The first is the understanding of the relation between the Hong Kong terrain and airflows. The three major mountain chains (Tai Mo Shan-Sunset Peak, Lion Rock-Ma On Shan, and Mount Parker-Victoria Peak) in Hong Kong roughly form an east-west ventilation corridor, within which the most densely populated urban zone is situated. Subsequently, the horizontal advection from the zonal winds is an effective mechanism to disperse pollutants horizontally. When the boundary layer wind has a strong meridional component, the mountain chains shelter the urban zones and allow the pollutants to accumulate at the surface. Moreover, the complex terrain of Hong Kong creates six air sheds (see Planning Department, 1993) in which concentrations of air pollutants become higher than those in the more open areas. Second, although the synoptic situations are still dominant factors for air pollutant dispersal, forecasters need to recognize when the local forcing mechanisms become dominant. For instance, when the winter surface winds are calm and the subsidence is strong under a quasi-stationary high surface pressure system, solar heating at the surface will become the only dominant forcing mechanism in the air pollution forecast. As discussed earlier, solar heating at the surface will promote the growth of the boundary layer. As the boundary layer grows deeper, the vertical turbulent mixing process will dilute the concentration of the surface air pollutants. When air pollutants are transported to a higher altitude (this is particularly true if the boundary layer top grows above the height of the local mountains), the horizontal advection process can become more effective in the dispersal of air pollutants because the wind speed generally increases with height. Moreover, differential surface heating will also generate local circulations, which will help ventilate local air pollutants (Wai *et al.*, 1996). Therefore, the prediction of the growth of the boundary layer and local circulations are important to predict when the concentration of air pollutants either reaches an unacceptable level or begins to subside.

In the site-specific air pollution forecast, the spatial scale is of the order of 1 km. If we take the boundary layer wind as 5 m s^{-1}, the time scale is thus of the order of 1 minute. Detecting the pollutants under this situation is therefore nearly instantaneous. Air pollutant dispersion is by turbulence processes and so the height of the boundary layer, the height of the emissive source, and the surface roughness (given by the height of building) are all important parameters in forecasting the dispersing processes on this scale.

Acknowledgements

The author thanks the staff at the Hong Kong Observatory and the Hong Kong Environmental Protection Department for the revised maps of Hong Kong weather stations, radiosonde data, and air quality data. In particular, the author gratefully acknowledges the help from Mr. K. P. Wong and M. C. Ng at the Hong Kong Observatory, Mr. T. C. Cheng, Mr. M. M. Yeung, and Mr. Tony Lam at the Hong Kong Environmental Protection Department.

References

Chen, J.C., S. C. Kot, and J. M. Tepper (1996) Detecting inversion and stable lapse rates with RASS. *Bull. H. K. Meteor. Soc.*, **6**, 13-20.

Hsu S.I. (1985) *Environmental problems of the development of the Shenzhen Special Economic Zone.* Occasional Paper No. 50, Department of Geography, The Chinese University of Hong Kong, Hong Kong. 19 pp.

Hunt, J. C. R. (1981) Diffusion in the stable boundary layer. *in* Nieuwstadt, F. T. M and H. Van Dop (Eds.), *Atmospheric Turbulence and Air Pollution Modelling*, Reidel, Dordrecht, 358 pp.

Koo, E., B. Y. Lee, and C. M. Tam (1984) *Meteorological studies of the Junk Bay air shed.* Occasional Paper No. 61, Royal Observatory, Hong Kong, 52 pp.

Lamb, R.G. (1981) Diffusion in the convective boundary layer. *in* Nieuwstadt, F. T. M and H. Van Dop (Eds.), *Atmospheric Turbulence and Air Pollution Modelling*, Reidel, Dordrecht, 358 pp.

Nai-Ling, L., W. D. Neff, and J. C. Kaimal (1983) Wave and turbulence structure in a disturbed nocturnal inversion. *Boundary-Layer Meteor.* **26**, 1412-15.

Planning Department (1993) *Territorial development strategy review environmental baseline conditions.* Hong Kong Government, Hong Kong. 124 pp.

Planning Department (1996) *Consolidated technical report on the territorial development strategy review* Hong Kong Government, Hong Kong. 179 pp.

Szepesi, D.J. (1987) *Applications of meteorological atmospheric pollution problems.* Technical Note No. 188, World Meteorological Organization, Geneva. 51 pp.

Wai, M.M.K., E.A. Smith, P. Bessemoulin, A. D. Gulf, A. J. Dolman, and T. Lebel (1997) Variability in boundary layer structure during HAPEX-Sahel wet-dry season transition. *J. Hydrology*, **188-189**, 965-997.

Wai, M.M.K., P.T. Welsh, and W.M. Ma (1995) The timing and distribution of summer convective rainfall over Hong Kong and South China. *Bull. H. K. Meteor. Soc.*, **5**, 3-20.

Yeung, K.K., W.L. Chang, B.Wan, F. Kimura and T. Yoshikawa (1991) Simulation of boundary layer flow in Hong Kong. *Atmos. Environ.* **25A**, 2161-2172.

Mickey M.K. Wai

Plum Rain Solutions, 2019 Skyland Drive, Tallahassee, FL 32303, USA

Changes in the Characteristics of Typhoons Affecting Hong Kong, Part 1: Typhoon Intensity in the South China Sea

Abstract

The climatological typhoon tracks are used to obtain useful insights into the changes of typhoon intensity and areas of origin of typhoons that affect Hong Kong. There are two areas of origin of typhoons in Hong Kong: within a belt of 10 degrees centered over the mean surface monsoonal trough and over a region near 15 °N and 115 °E in the South China Sea. In terms of storm intensity, the storms are divided into two groups: weak storm (less than 60 kts) and strong storm (greater than 60 kts). The tracks are grouped into three regions: Luzon Island, Bashi-Balintang Channel, and the South China Sea.

Roaring into the South China Sea across Luzon Island along a southeast-northwestern track, the mean storm intensity is reduced from 100 kts to 50 kts within 48 hours after entering the South China Sea. Along a similar southeast-northwestern track over the Bashi-Balintang Channel, the mean storm intensity is lowered from 110 kts to 35 kts in 48 hours. On the contrary, weaker storms strengthen from 30 kts to 45 kts after crossing over Luzon Island and passing through theBashi-Balintang Channel along a similar southeast-northwestern track into the South China Sea. When the storms pass over the central Philippines into the South China Sea, the mixed underlying surfaces of water and islands do not affect the intensity of the storm. In this case, the storms can reach a severe tropical storm (60 kts) within 48 hours after entering the South China Sea. If the storms maintain an east-west track after crossing from Bashi-Balintang Channel to the South China Sea, the storms are reduced from 80 kts to 60 kts within 48 hours.

When the storms originate in the South China Sea, the tracks are either roughly in north-south or in erratic directions. In the north-south tracks, the storms will intensify but begin to fill about 24 hours prior to making landfall. With the erratic tracks such as looping, Hong Kong may experience more than one periods of intensified winds.

Introduction

The landscape of Hong Kong is comprised of water and 236 islands of which nearly 75 percent of the terrain is hilly. To meet the need of her citizens, the government of Hong Kong continuously seeks additional lands for the private, public and commercial sectors. The acquisition of additional lands is largely accomplished by

reclamation. Between 1976-1994, about 3000 hectares of coastal land were added to the Hong Kong area by reclamation. Current projects of reclamation along the waterfronts will last through the next decade.

As the hilly terrain is modified unnaturally and coastal lands are reclaimed, the risk of these new developments being exposed to weather or climatic change induced hazards will also increase. For instance, Yim (1996) discussed the vulnerability of Hong Kong to hazards under climatic change conditions. Since the records of typhoon signals began to be kept in 1946, Hong Kong Observatory (formerly known as Royal Observatory) has issued 807 typhoon warning signal No. 1 or higher by the end of 1999. About 25 percent of the warnings were typhoon signal No. 8 or higher. Therefore, a need for assessing the dangers associated with a typhoon, which either passes by Hong Kong within 800 km or makes landfall, has become more pressing than ever. The potential threats underscore the need for adequately understanding the impact of the high winds, storm surge, flooding, and possible landslide associated with a typhoon. An important step in understanding the impact of a typhoon is to study the change in the intensity as a typhoon approaches Hong Kong.

The optimal approach to predict the intensity and the life cycle of a typhoon is to utilize a numerical weather prediction model. The current abilities to predict the intensity and the potential damage of a typhoon with the most advanced numerical weather prediction models are limited. Moreover, viewpoints are divided on a number of physical processes, which are thought to be responsible for the changes in the intensity of a typhoon (Elsberry, 1992). In addition to the uncertainty, recent observations (Simpson *et al.*, 1997) appear to support the hypothesis that thegenesis and track of a typhoon should not be treated as a deterministic or initial value problem (Ooyama, 1982). Therefore, a statistic or chaos approach is needed because of the nonlinear interaction of widely differing spatial scales. Since the numerical models have limitations, it has therefore become necessary to develop objective guidance tools from climatological data. In South China Sea and western North Pacific Ocean, Chin (1958) documented the typhoon climatology from 1884 to 1953 and from which Chin obtained the frequency of occurrence, frequency distributions of speed of motion and direction of motion. Also in an updated report, Chin (1972) included the tracks of typhoons from 1954 to 1970. All these statistics were given in charts and diagrams. The discussion of the climatology of typhoons between 1884-1964 was given by Pun (1966). More recently, Fok (1997) presented a climatological survey of the origin, dissipation, path, and frequency of typhoons between 1966-1995. The analyses of typhoon climatology have led to useful knowledge for many applications such as the design of an engineering project and mapping the shipping routes. For forecasting, their usefulness is limited because those studies do not consider environmental or meteorological variables from which one can form the basis of guidance for the forecasters. Moreover, not all typhoons which form either in the South China Sea or in the western North Pacific Ocean will affect Hong Kong. Therefore, it has become necessary to include the key mechanisms that control the intensity changes of a typhoon and to consider the interaction between the typhoon and the large-scale environments.

It is accepted that a typhoon itself is a complete system. An example of its components is illustrated in Elsberry *et al.* (1992). In simple terms, a typhoon can be thought of as a heat engine, which consists of a fuel tank (ocean), cylinders (eyewall convection), and exhaust pipes (upper-troposphere outflow). The meteorological variables associated with the heat engine are sea surface temperature, relative humidity in the mid-troposphere, vertical gradient of equivalent potential temperature, vertical wind shear, low-level relative vorticity, the Coriolis parameter, and eddy flux momentum convergence at 200 hPa. The first three are thermodynamical variables while the others are dynamic variables.

The thermodynamical variables vary slowly with seasons, and they are difficult to use in distinguishing a developing typhoon from a non-developing typhoon in a daily forecast. Therefore, dynamical variables are more useful in day to day forecast but the observations are not always available over the ocean. We need to rely on other techniques to provide supplemental guidance to forecasters.

Since a large majority of typhoons form at a distance of more than 1000 km from Hong Kong, and even some typhoons develop over the South China Sea, the advanced remote sensing satellite generally enables the forecaster to detect the early development of a typhoon. Therefore, the accurate forecast of the formation of a typhoon becomes less critical in terms of the readiness of the approach of a typhoon.

The accuracy of typhoon intensity changes and motion forecasts are equally important to the users during the life cycle of a typhoon. Wang *et al.* (1998) and Dong (1988) have discussed the dynamical influences on the motion of tropical cyclones. In terms of difficulty, forecasts of intensity changes of a typhoon are considered more difficult than forecasts of typhoon motion. It is because the atmospheric processes that determine the major portion of typhoon motion are of large scale but overall are not complex. In contrast, the typhoon intensity changes are governed by the complex physical processes which are of multiple and smaller scales. Furthermore, the initial intensity of a typhoon is not observed with a sufficient degree of accuracy.

Moreover, there is no correlation between the occurrence of warning signals raised in Hong Kong as an indication of proximity of typhoons and the actual proximity of typhoons (Jeary, 1997). As will be shown later in this paper, when the typhoons enter the South China Sea, the typhoons will affect Hong Kong to varying degrees. Consequently, the forecast of intensity changes of an approaching typhoon is more critical than the forecast of the formation and the motion of typhoon.

Objectives of Study

The study has four objectives. The first objective is to determine what meteorological variables are relevant to the formation and intensity changes of a typhoon with respective to Hong Kong. This is accomplished by re-examining a number of physical processes that are thought to be important in the life cycle of a typhoon. The second objective is to link the points of origin of typhoons to the environmental or meteorological variables. In particular, special attention is focused on a group of typhoons that eventually affect Hong Kong. The third objective is to examine how the intensity of this selected group of typhoons changes after they sweep into the South China Sea. The fourth objective is to derive some guidelines that will provide forecasters with clues on the intensity changes when a typhoon is likely to affect Hong Kong.

Sea Surface Temperature (SST)

a. Maximum potential typhoon intensity

Early observational studies indicate that the typhoons tend to develop in areas of higher SST and to decay in areas of lower SST. For tropical cyclones to reach typhoon force, the SST needs to exceed 26 °C (Palmen 1956). This threshold is confirmed numerically by Ooyama (1969), Riehl (1979), Kuroda *et al.* (1998) among others. Furthermore, the intensification of a typhoon is likely to occur when the SST is warmer than 28 °C (Nyoumura and Yamashita, 1984).

To link the relationship between SST and the intensity of a typhoon, Merrill (1988) obtained graphically the maximum potential typhoon intensity by correlating both the maximum wind speed of a typhoon and the corresponding climatological SST to the frequency of occurrence of the typhoon. To confirm the maximum potential typhoon intensity, Emanuel (1988) derived a relation from which the maximum possible pressure deficit in the eye of a typhoon was given by the product of the latent heat from the ocean to the atmosphere and thermodynamic efficiency proportional to the temperature difference between the sea surface and lower stratosphere. Therefore, the maximum possible intensity attainable by a typhoon is linked to the sea surface temperature, and this relationship is presumed dominant over all other effects.

Two studies, one by Miller (1958) and the other by Merrill (1987), indicate that increasingly warmer seawater will provide fuel for stronger typhoons to form but the environmental factors other than SST are likely to be of equal or greater importance throughout the cyclone's life cycle. To clarify the actual role of SST in determining the maximum possible intensity of a typhoon, Evans (1993) examined a global set of tropical cyclones and monthly SST from 1967-1986 for the relationship between the maximum tropical cyclones intensity and SST. The analyses suggest that while tropical cyclones form preferably over warm

waters, SST alone is not a dominating factor in determining the actual maximum intensity attained by a tropical cyclone. A regional study of the western North Pacific storms from 1960 to 1990 using a similar approach to DeMaria and Kaplan (1994), Baik and Paek (1998) found that the Pacific storms seldom reach their maximum potential intensity for a given SST. In agreement with Evan's study, the environmental influences also appear to be important in determining the maximum intensity of the Pacific storms. Moreover, the yearly-average relative intensity shows little correlation either with quasi-biennial oscillation or with El Niño.

b. Feedback of SST on the typhoon intensity

During the genesis and developmental stage of a typhoon, warmer SST is a positive feedback in the typhoon-ocean system. As the typhoon strengthens, the evaporation rate grows due to the increase in the surface wind speed. The enhancement of the moisture supply from the ocean leads to the increase in the latent heat flux that drives the typhoon circulation.

As the typhoon moves away from the spawning warmer sea surface, it was once assumed that the sea surface temperature beneath the path of a typhoon does not change significantly. Therefore, it was thought that there is no negative feedback between the SST response and the typhoon intensity.

From observations of seven intense hurricanes, Jordan and Frank (1964) reported an averaged drop of SST of 0.5 °C. They also found that the maximum cooling occurred to right of the path, and the phenomenon was supported by other field studies (Federov *et al.*, 1979, Sanford *et al.*, 1987; Shay *et al.*, 1992; and Breaker *et al.*, 1994). The cooling by the surface evaporation was insignificant (Ramage, 1972).

The spatial variation of SST along the track of a typhoon is best revealed by the satellite images. The maximum cooling in the SST occurs to the right of the track of a fast moving typhoon (Stramma *et al.*, 1986), where upwelling causes negligible cooling at the sea surface. However, for a slow moving typhoon, the maximum cooling in the SST occurs near or on the track, where upwelling causes a significant lowering of the SST. The cooler SST following the passage of a typhoon can last from a few days to at least 16 days. The amplitude of cooling is moderately correlated with the strength of a typhoon. The SST difference can be as large as 3.5 °C. However, the local hydrographical condition in slope water can make the sea surface cooling up to 9 °C (Sakaida, 1998).

The typhoon circulation can lower the surface SST beneath its path. A small or even a negative sea-air temperature difference will reduce the sensible and latent heat fluxes necessary to sustain the typhoon intensity. Subsequently, the typhoon circulation and the intensity will be weakened.

Low-level Relative Vorticity

Tropical cloud clusters that develop into tropical storms are always found in regions of low-level positive vorticity. Such regions include ITCZ, monsoon trough, and near equatorial trough.

In the western North Pacific, the surface monsoon trough, a prominent feature, is oriented from northwest to southeast direction during the summer months. Along the surface monsoon trough, enhancement of low-level flow on either side of the monsoon trough increases the positive vorticity, and moisture concentration that make the meteorological conditions favorable for the typhoon formation.

As the southwest monsoon strengthens, the surface monsoon trough undergoes latitudinal migration during the typhoon season. From early to mid typhoon seasons, the surface monsoon trough moves northward to around 25° N by August. Towards the end of November, the surface monsoon trough recedes southward to about 5° N. In late typhoon season, the mean surface monsoon trough is aligned in a more east-west direction. While the mean surface monsoon trough does not go beyond 130° or 140°E in the original analysis, the surface monsoon trough can have extended further eastward as indicated by the spatial distribution of the typhoons and the values of directional shear.

The surface monsoon trough has been noted to be associated with about 80 percent of typhoon formation in the west Northern Pacific. Using the satellite images, Zehr (1992) describes a two-stage process how the surge associated with the surface monsoon trough initiates the formation of a typhoon. The linkage of the surface monsoon trough to the formation of a typhoon was also noted in the studies of the tropical cyclones over Guam (NOCC/JTWC, 1991) and the relationship between tropical storm formation in the western North Pacific and ENSO (Lander, 1994). For instance, in the case of typhoon Oliver, observations indicated that the low level vertical wind shear over the mesoscale convective vortex enables the development of the large mesoscale system in the vicinity of a surface monsoon trough (Simpson *et al.*, 1997). The gradual strengthening of the surface monsoon trough leads to the increase of cyclonic vorticity in low and mid-levels, and associated reduction of the deformation radius which suppresses the gravity waves and allows convective heating to be transferred to local rotation and vortex to spin up.

Interaction with a Land Barrier

a. Intensity changes and track deflection

A subtle situation occurs when a typhoon approaches and crosses over an island. An earlier study indicates that the average intensity of typhoons decreases by 33 percent when moving across the Philippines (Brand and Blelloch, 1973). The decrease in the intensity is noted about 24 hours prior to the crossing of the Philippines. Track deflection is also found over Philippines (Shoemaker, 1991) and Taiwan (Brand and Blelloch, 1974). However, the track deflection is the greatest over Taiwan when it is compared to the Philippines. The mountain terrain of Taiwan also produces a secondary low on the lee side of Taiwan (Hsu, 1960).

b. Landfall

In a landfall situation, the finite heat capacity and conductivity of the soil lower the land surface temperature, and the subsequent reduction of surface evaporation. The surface roughness and wetness at the land surface bring lower wind speed. Therefore, lower wind speed and reduction of surface evaporation lead to rapidly filling of a tropical cyclone (Tuleya, 1994).

The shape of the coastline can influence the rate of filling of a typhoon during landfall. Along the U.S. Atlantic coast, strong storms (46-63 kts) and weak hurricane (64-83 kts) fill both more rapidly and by a greater amount over concave coasts than they do over convex coasts (Rogers and Davis, 1993). This is probably because the land to ocean ratio is larger in a concave coast where the reduction of both latent and sensible heat fluxes from the surface are larger than those in the convex coast line. If the intensity of a storm is considered, stronger storms fill more rapidly than the weaker storms in regardless of the coastline curvature.

Upper Level Trough

a. Western North Pacific Ocean

During the late typhoon season, a very extensive cloud plume consisting of middle and high cloud stretched northeastward from the center of a named typhoon (Erickson and Winston, 1972). Such cloud plumes were shown to be responsible for transporting tropical heat and moisture to the westerlies. The development of the cloud plume outflow aloft was caused by the divergence of heat flux ahead of an approaching westerly upper-level trough (Ramage, 1974). Furthermore, the vorticity advection east of the trough line enhanced mass divergence above the typhoons, the winds of which also intensified at the time of the cloud plume formation.

It is noted that the mid-latitude Westerlies seldom extend into the tropical western North Pacific Ocean in early and mid-typhoon seasons. Moreover, Sadler (1976, 1978) noted the Tropical Upper Tropospheric

Trough (TUTT) from the synoptic analysis of tropical circulations at 200 hPa. Therefore, Sadler recognizes that the TUTT may act like the mid-latitude westerlies. Here, the TUTT is a rather small and tight feature. The monthly location of the TUTT tends to be diffused. In early typhoon season, the mean TUTT is located north of 15° latitude. When the typhoon season progresses to mid-season, the mean TUTT migrates northward to 20° N. As the typhoon season comes to end, the mean TUTT shifts back to 15° N.

Because the TUTT is found in the vicinity of a developing typhoon, Sadler proposed that the TUTT is the outflow feature to export mass and heat to the westerlies at the upper level by increased convection in the developing depression. Moreover, the location of the TUTT over the low-level trough tends to decrease the vertical wind shear.

Examinations of typhoon development from satellite images do not support the dominant role of the TUTT in the formation of typhoons in the western North Pacific. In his study of 1983-1984 satellite images of typhoons, Zehr (1992) examined the locations of the storms with respective to the axis of the TUTT. In 42 cases of Stage 1 pre-tropical storm, 61 percent lay within 20 degrees of latitude of the TUTT axis. Similarly, in 51 cases of Stage 2 pre-tropical storm, 55 percent lay within 20 degrees of latitude of the TUTT axis. When the same analysis was done with the 22 non-developing disturbances, at the time of the nearest maximum convection, 68 percent were associated with the TUTT. When the distance criteria is reduced to 10 degrees of latitude, the percentages are decreased to less than 40 percent for both non-developing and the pre-tropical storm disturbances. The results suggest that a typhoon can form without the assistance of the TUTT (Zehr, 1992).

The wind analysis at the 200 hPa level suggested that divergence played a passive role in the formation of typhoon (Zehr, 1992). The upper level divergence appears to occur mostly in response to low-level convergence and to active convective areas, rather than vice-versa. Moreover, the upper relative vorticity associated with non-developing and pre-typhoon disturbance tends to be negative. Therefore, upper-level vorticity differences do not appear to play an important role in the formation of typhoons.

The response of a typhoon at the upper level to the forcing at the lower level is described in a study between the surface wind intensification and cloud plumes aloft from 25 autumn typhoons between 1967-1974 (Tsui *et al.*, 1977). In 16 cases, enhancement of heat outflow occurs after the intensification of surface wind speed. In 5 cases, the surface winds decrease before the upper-level cloud plume is observed while in the remaining four cases, surface winds do not change before the observation of the upper-level cloud plumes. During the subsequent 24 hours, after the cloud plume is observed, there is almost an equal chance of intensification or weakening in the surface wind.

b. North Atlantic Ocean and Caribbean Basins

A numerical study shows that upper-level momentum fluxes can intensify a vortex (Pfeffer and Challa, 1981), and the final wind field around the vortex resembles a hurricane wind force. Two other case studies show that upper level eddy momentum fluxes are important for the intensification of the storm (Molinari and Vollaro (1989,1990). However, in a 5-year composite of the Atlantic hurricanes, Merill (1988) finds no clear relationship between intensity change and eddy momentum fluxes. Since large eddy momentum fluxes are often associated with the interaction between an upper level trough and a storm, Merill (1988) suggests that the positive influence of eddy momentum flux may be compensated by the negative influences of increased vertical wind shear associated with the upper-level trough.

To examine the role of the upper level trough on the intensification of a typhoon, DeMaria *et al.* (1993) studied the named Atlantic typhoons in the 1988-1991 hurricane seasons. In about one-third of the cases, the storm intensifies just after a period of increased eddy flux convergence. In most of the cases when the storms do not intensify, the vertical wind shear increases, or the storm moves over cold water, or the storm becomes extratropical just after a period of increased eddy flux convergence. Therefore, the eddy momentum flux associated with the upper level trough can fuel or inhabit the intensification of a typhoon. The strong vertical wind shear negatively influences the intensification of a tropical cyclone, which is also consistent with Gray's study (Gray, 1998).

In the rapidly intensifying cases, the eddy flux convergence is large but the vertical wind shear is low in six out of ten cases. Furthermore, the 200 hPa analyses show that the storms are on the edge of the upper level cyclonic features, but the storms never move directly beneath them. In the remaining four cases, the storms intensify rapidly in a low vertical wind shear without any obvious interaction with the upper level trough. Therefore, the orientation of the upper level cyclonic feature relative to the storm is a critical factor for determining whether the eddy momentum fluxes in the upper level trough will intensify a typhoon. Similar relationships between the eddy momentum fluxes and the intensity change of a storm are also shown by the diagnostic study of typhoon Flo and typhoon Gen (Wu and Cheng, 1999) and a numerical study of typhoon Tip and tropical depression Faye (Challa, *et al.*, 1998).

Data

Both observations and diagnostic studies indicate that both sea surface temperature and vertical shear are important variables in the formation and the intensity changes of a typhoon. In the western North Pacific, the surface monsoon trough and its associated low level vorticity are important in the genesis of a typhoon. As the typhoons cross a land mass or makes landfall, surface friction and the reduction in the moisture spin it down. Therefore, one can establish some relationship between the changes in the typhoon intensity and the SST, vertical wind shear, and land barriers by analyzing the typhoon tracks.

The primary typhoon track data from 1954 to 1999 are acquired from the Joint Typhoon Warning Center, Honolulu, Hawaii. Typhoon tracks prior to 1954 are based on two volumes of typhoon climatology from 1884 to 1958 (Chin, 1958) and from 1959 to 1972 (Chin, 1972) published by the Hong Kong Observatory. Additional typhoon tracks are supplemented from a series of tropical cyclone summaries published in the *Hong Kong Meteorological Society Bulletin* from 1991 to 1998 (for example, Kyle, 1999), published by the Hong Kong Meteorological Society.

Table 1. Names of upper air stations

ID	Station Name	Latitude	Longitude
47909	Naze	28 23 N	129 33 E
47931	Kadena, Okinawa	26 21 N	127 45 E
91115	Iwo Jima	24 47 N	141 20 E
91131	Marcus Island	24 17 N	153 58 E
45004	Hong Kong	22 19 N	114 10 E
98327	Clark Air Base, Philippines	15 10 N	120 34 E
91218	Guam	13 34 N	144 55 E
91250	Eniwetok Atoll	11 20 N	162 20 E
91413	Yap	09 31 N	138 08 E
91366	Kwajalein	08 43 N	167 44 E
91334	Truk, Caroline Islands	07 27 N	151 50 E
91408	Koror, Palau	07 21 N	134 29 E
91348	Ponape	06 58 N	158 13 E
96481	Tawau, Malaysia	04 16 N	117 53 E
96441	Kota Kinabalu, Malaysia	03 12 N	113 02 E
96413	Kuching, Malaysia	01 29 N	110 20 E

The SST patterns in the western North Pacific Ocean are based on Oceanographic Monthly Summary (1981-1991) and Climate Diagnostic Bulletin (1992-1994). Additional SST in the South China Sea is provided by Wong's analysis (1979). The vertical horizontal wind shear between 850 and 300 hPa in the western North Pacific and in the South China Sea are calculated from a data set of upper wind climatology published by AWS/USAF (1961). Additional upper air soundings are obtained from the Climatological data of the World. The names of the upper air stations used are listed in Table 1 and their locations shown in Figure 1.

Figure 1. **Location of upper air stations.**

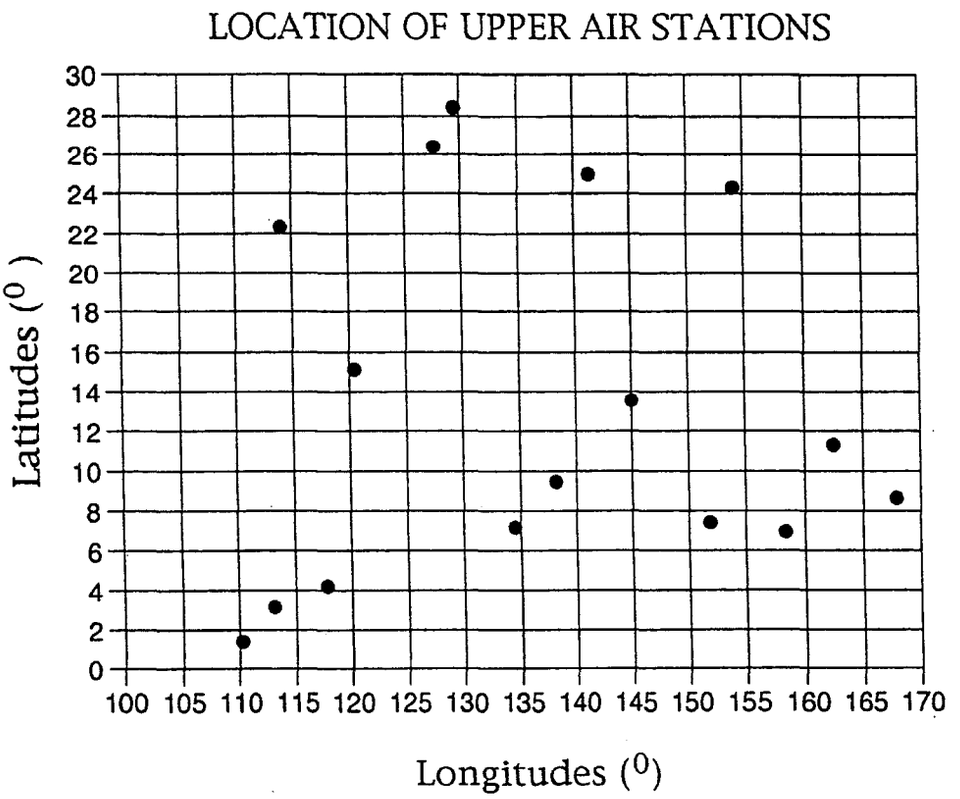

To illustrate the relative positions of the TUTT with respective to the origins of typhoons, the positions of the TUTT are obtained from the Analysis of the Upper Tropospheric Circulation over the Tropics (Sadler, 1975). The positions of the surface monsoon trough during the typhoon season are based on the analyses of tropical winds (Atkinson, 1970) and tropical circulation and cloudiness (Sadler and Harris, 1970).

Patterns of Large-Scale Environments

a. Sea surface temperatures

Three horizontal profiles of SST across the western North Pacific Ocean are shown in Figure 2. The meridional SST pattern along 114 °E (the top panel) remains around 29.8 °C in the equatorial tropics until it reaches around 12 °N. Further to the north over the continental shelf, the SST decreases to 28.2 °C at 22 °N. The continental shelf water is cooler than the interior South China Sea.

Figure 2. Cross sections of mean summer SST (°C) in the western North Pacific Ocean. (a) Along 114 °E. (b) Along 20 °N. (c) Along 10 °N, 140 °E and 23 °N, 114 °E.

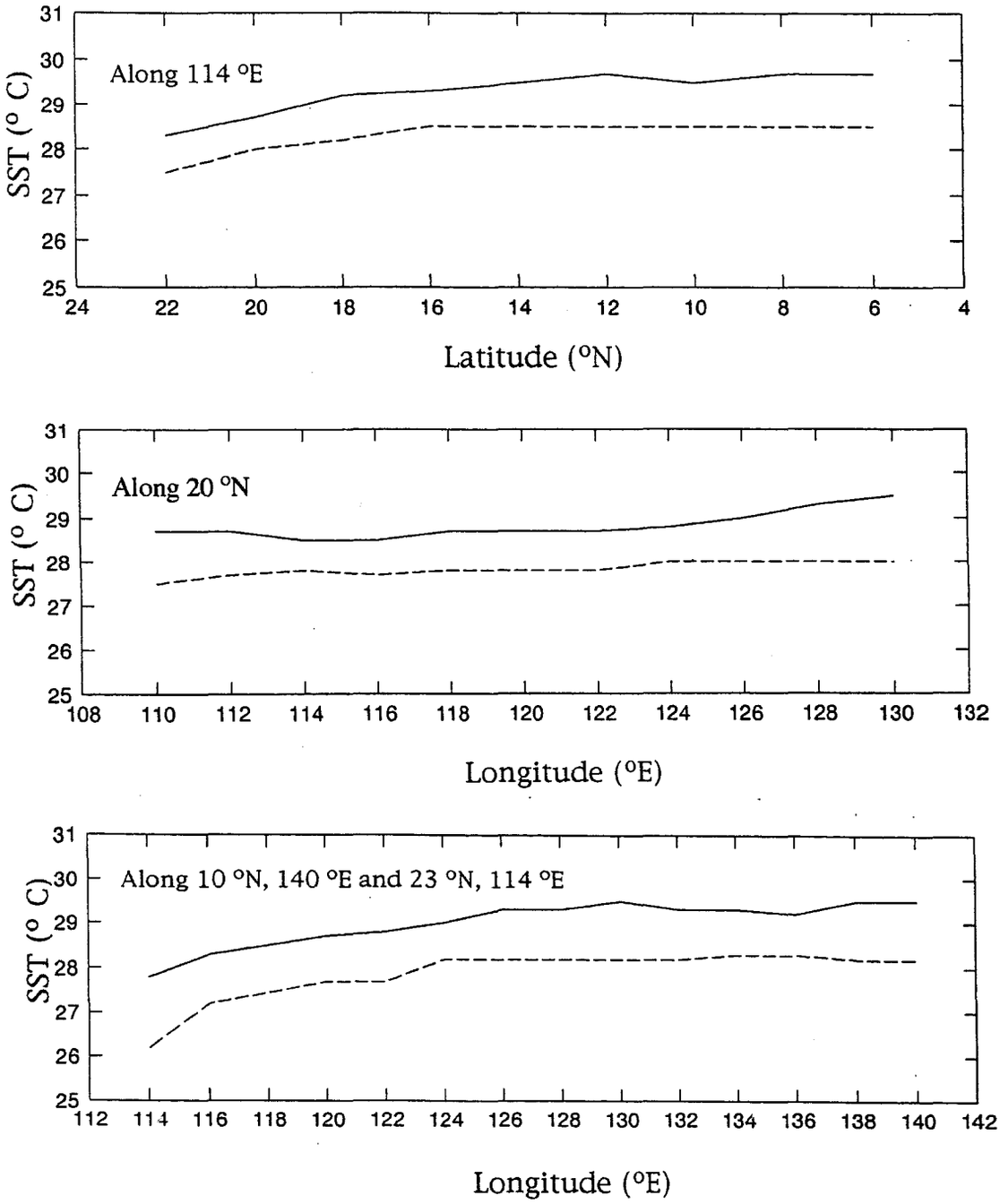

When moving westwards horizontally through the Bashi-Balintang Channel along 20 °N (the middle panel), the SST decreases from 29.6 °C to a relatively minimum of 28.3 °C in the interior of the South China Sea. Similarly, along the southeast-northwest direction from 10 °N and 140 °E to 23 °N and 114 °E, the SST decreases from 29 °C in the Pacific to a temperature below 28 °C in the South China Sea. The large-scale SST pattern shows the highest SST in the southwest equatorial North Pacific Ocean. Because of minimum mixing between western North Pacific Ocean and South China Sea, the SST in the South China Sea is cooler than the western North Pacific Ocean by 1 to 1.5 °C.

b. Vertical shear of horizontal winds

The forecasters at JTWC consider the large-scale wind a favorable condition for typhoon formation and intensification when the directional shear of horizontal wind vectors between 300 hPa and the surface is smaller than 45 degrees and the corresponding magnitude of the vertical shear is less than 15 kts. Because the upper wind climatology did not include the surface wind vectors, the vertical shear is calculated between 300 and 850 hPa in this study.

The monthly values of the vertical shear are smaller than 15 kts. However, the values of the directional shear and their patterns show both seasonal and spatial variations. Therefore, a summary of this monthly directional shear is shown in Tables 2 to 4.

Table 2. **Spatial patterns of vertical wind direction shear between 850 and 300 hPa in degrees for the months of June and July.**

JUN

	110 – 115 E	115 – 120 E	120 – 125 E	125 – 130 E	130 – 135 E	135 – 140 E	140 – 145 E	145 – 150 E	150 – 155 E	155 – 160 E	160 – 165 E	165 – 170 E
30 – 32 N												
28 – 30 N				30								
26 – 28 N				46								
24 – 26 N							37		68			
22 – 24 N	135											
20 – 22 N												
18 – 20 N												20
16 – 18 N												
14 – 16 N			98									
12 – 14 N							25					
10 – 12 N												
8 – 10 N						4						150
6 – 8 N					6				28	35		
4 – 6 N		135										
2 – 4 N	168											
0 – 2 N	157											

JUL

	110 – 115 E	115 – 120 E	120 – 125 E	125 – 130 E	130 – 135 E	135 – 140 E	140 – 145 E	145 – 150 E	150 – 155 E	155 – 160 E	160 – 165 E	165 – 170 E
30 – 32 N												
28 – 30 N				160								
26 – 28 N				120								
24 – 26 N							109		100			
22 – 24 N	89											
20 – 22 N												
18 – 20 N												179
16 – 18 N												
14 – 16 N			94									
12 – 14 N							25					
10 – 12 N												
8 – 10 N						17						30
6 – 8 N					59				1	2		
4 – 6 N		148										
2 – 4 N	168											
0 – 2 N	158											

In June, the directional shear in the South China Sea is larger than 45 degrees. In the western North Pacific, a band of smaller values of directional shear less than 45 degrees is located near 12 °N. In July, a sharper spatial gradient of direction shear is found. The values of directional shear in the South China Sea remain high. In the western North Pacific, a NW-SE boundary, which extends from 26 °N and 110 °E to 18 °N and 170 °E, separates the interior of smaller values of directional shear from the higher values to the north.

Table 3. **Same as Table 2 except for the months of August and September.**

AUG

	110–115 E	115–120 E	120–125 E	125–130 E	130–135 E	135–140 E	140–145 E	145–150 E	150–155 E	155–160 E	160–165 E	165–170 E
30–32 N												
28–30 N				103								
26–28 N				76								
24–26 N							61		72			
22–24 N	42											
20–22 N												
18–20 N												160
16–18 N												
14–16 N			155									
12–14 N							35					
10–12 N												
8–10 N						82						3
6–8 N					150				21	6		
4–6 N		128										
2–4 N	150											
0–2 N	133											

SEP

	110–115 E	115–120 E	120–125 E	125–130 E	130–135 E	135–140 E	140–145 E	145–150 E	150–155 E	155–160 E	160–165 E	165–170 E
30–32 N												
28–30 N				140								
26–28 N				157								
24–26 N							29		32			
22–24 N	9											
20–22 N												
18–20 N												80
16–18 N												
14–16 N			115									
12–14 N							40					
10–12 N												
8–10 N						87						6
6–8 N					132				33	4		
4–6 N		178										
2–4 N	149											
0–2 N	117											

In August and September, the area of smaller values of directional shear extends into 25 °N. In the South China Sea, the interior directional shear becomes smaller even though they remain high to the south and southeast. When October comes, the larger values of directional shear near 25 °N return, indicating that the westerly trough penetrates southward into the tropics. Toward the end of November, a pattern of sharper spatial gradient returns.

Table 4. Same as Table 2 except for the months of October and November.

OCT

	110–115 E	115–120 E	120–125 E	125–130 E	130–135 E	135–140 E	140–145 E	145–150 E	150–155 E	155–160 E	160–165 E	165–170 E
30–32 N												
28–30 N				82								
26–28 N				144								
24–26 N							110		28			
22–24 N	140											
20–22 N												
18–20 N												100
16–18 N												
14–16 N			8									
12–14 N							16					
10–12 N												
8–10 N						67						2
6–8 N					167				22	19		
4–6 N		136										
2–4 N	139											
0–2 N	125											

NOV

	110–115 E	115–120 E	120–125 E	125–130 E	130–135 E	135–140 E	140–145 E	145–150 E	150–155 E	155–160 E	160–165 E	165–170 E
30–32 N												
28–30 N				172								
26–28 N				110								
24–26 N							106		146			
22–24 N	150											
20–22 N												
18–20 N												65
16–18 N												
14–16 N			32									
12–14 N							13					
10–12 N												
8–10 N						6						158
6–8 N					86				8	10		
4–6 N		68										
2–4 N	118											
0–2 N	116											

Points of Origin of Typhoons Affecting Hong Kong

Figures 3 to 5 show the origins of the typhoon in the western North Pacific between June and November from 1884 to 1999. Superimposed on these diagrams are the monthly mean positions of the surface monsoon trough (triangle symbols) and the TUTT (inverted triangle symbols). The dark circles indicate the typhoons, which affected Hong Kong between 1959 and 1999. The diamond symbols refer to those typhoons that make landfall in South China. The location of Hong Kong is marked by a dark diamond symbol.

Figure 3. Origin of typhoons in the western North Pacific for the months of (a) June, and (b) July. Surface monsoonal trough is represented by the symbol triangles. TUTT is indicated by the inverted triangles. Open circles are the origin of typhoons. Dark circles are the typhoons that affect Hong Kong. Symbol diamonds are the typhoons making land fall in South China. Hong Kong is marked by a dark diamond.

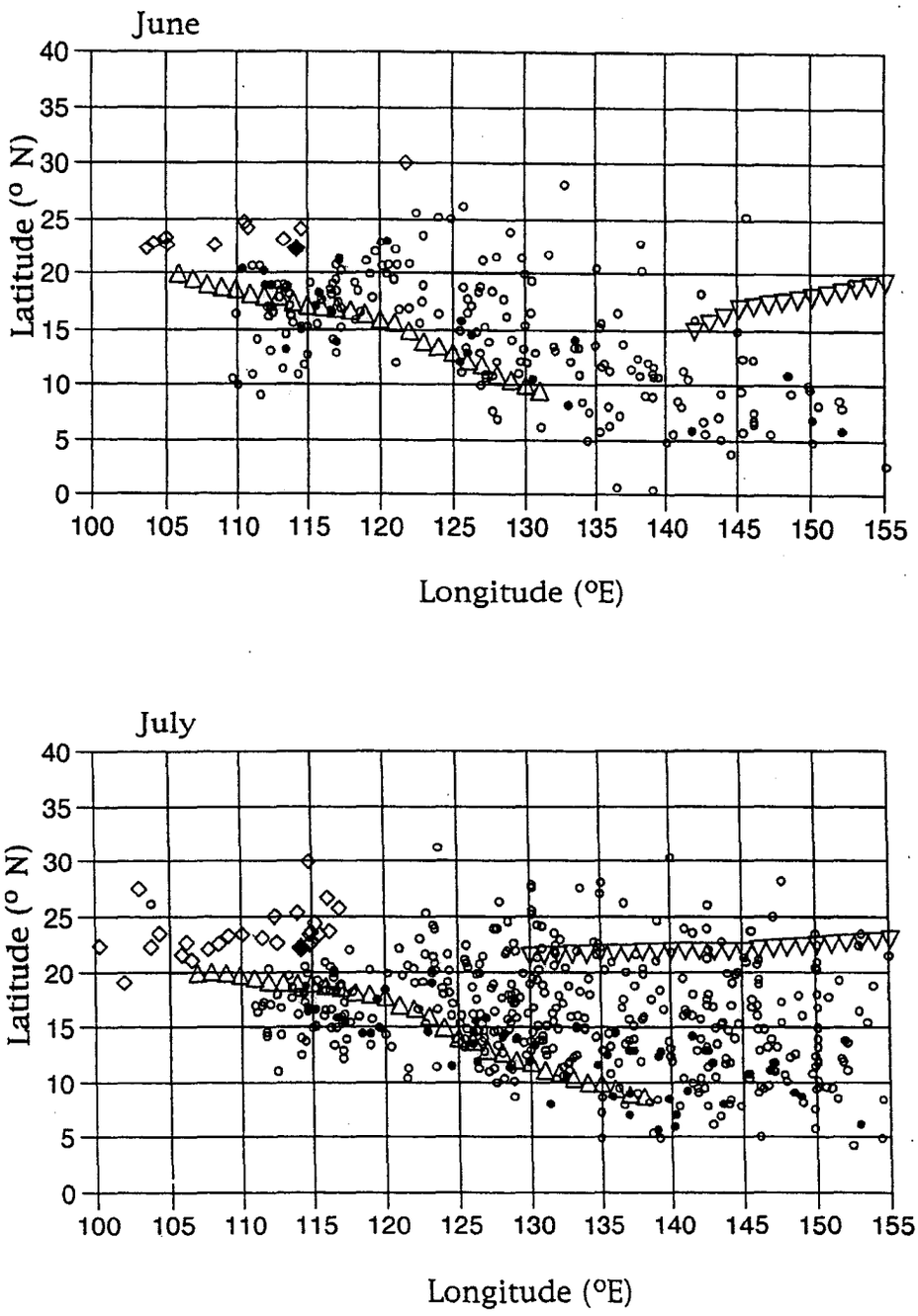

Figure 4. Same as Figure 3 except for the months of (a) August, and (b) September.

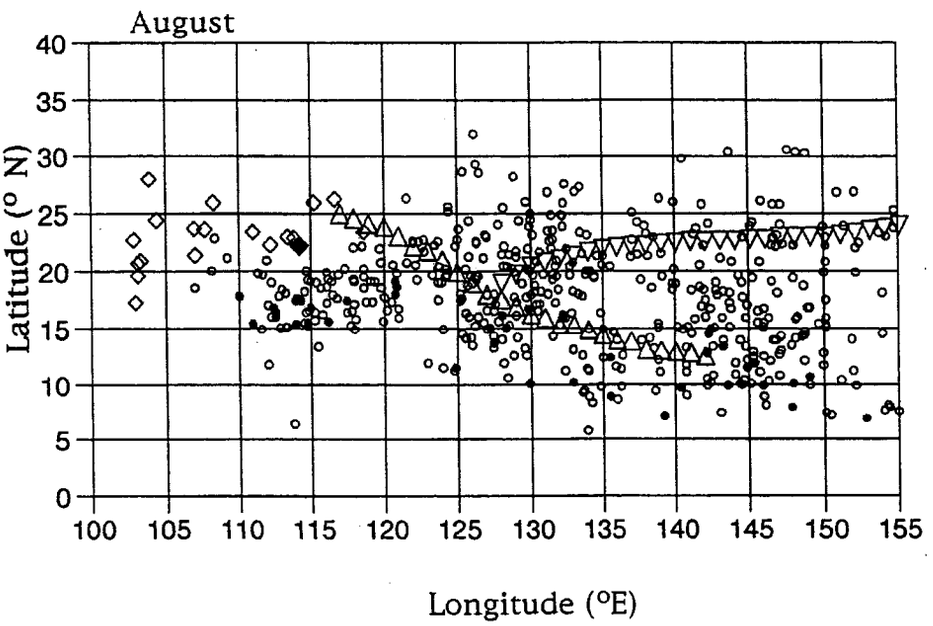

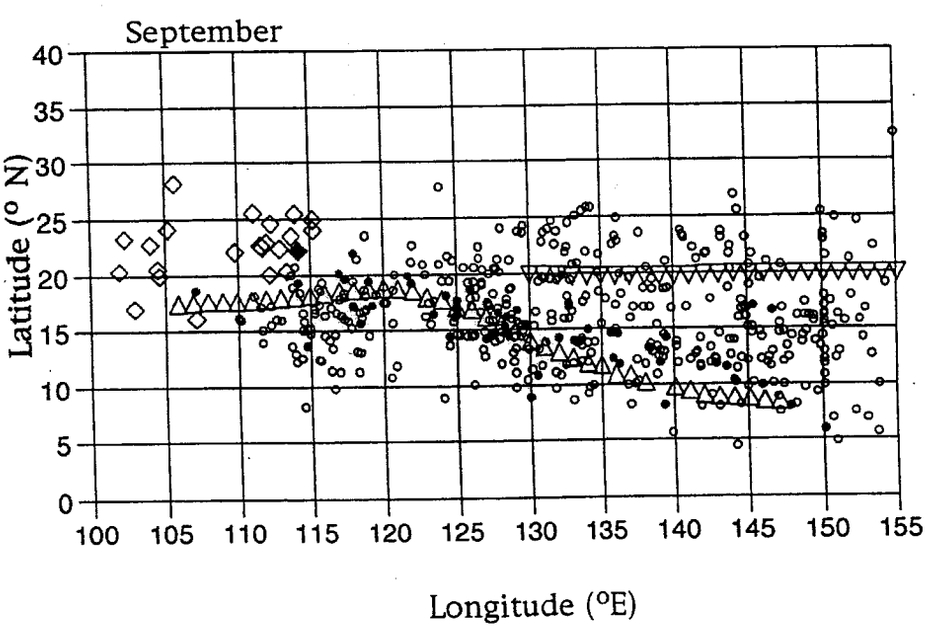

Figure 5. Same as Figure 3 except for the months of (a) October, and (b) November.

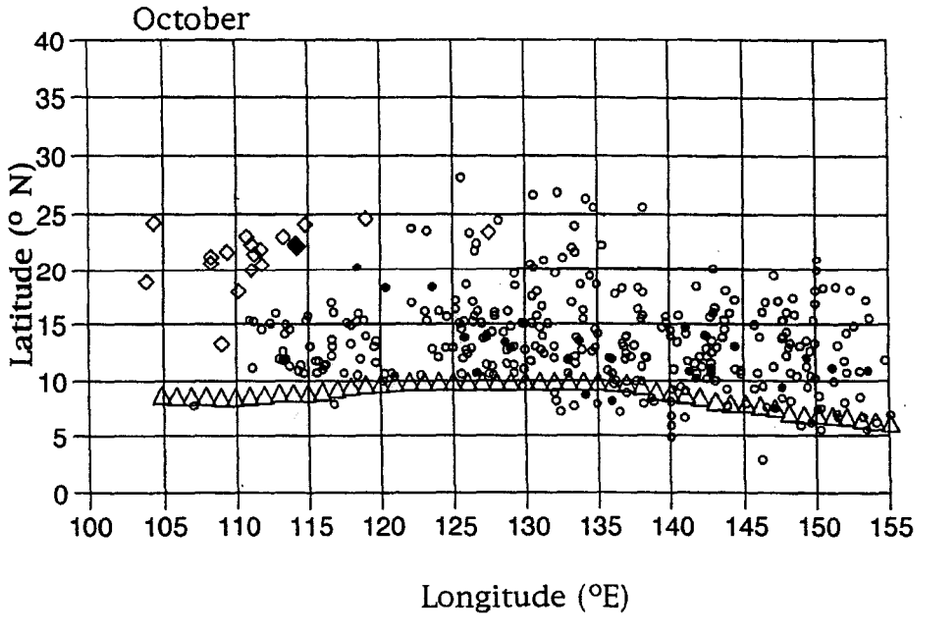

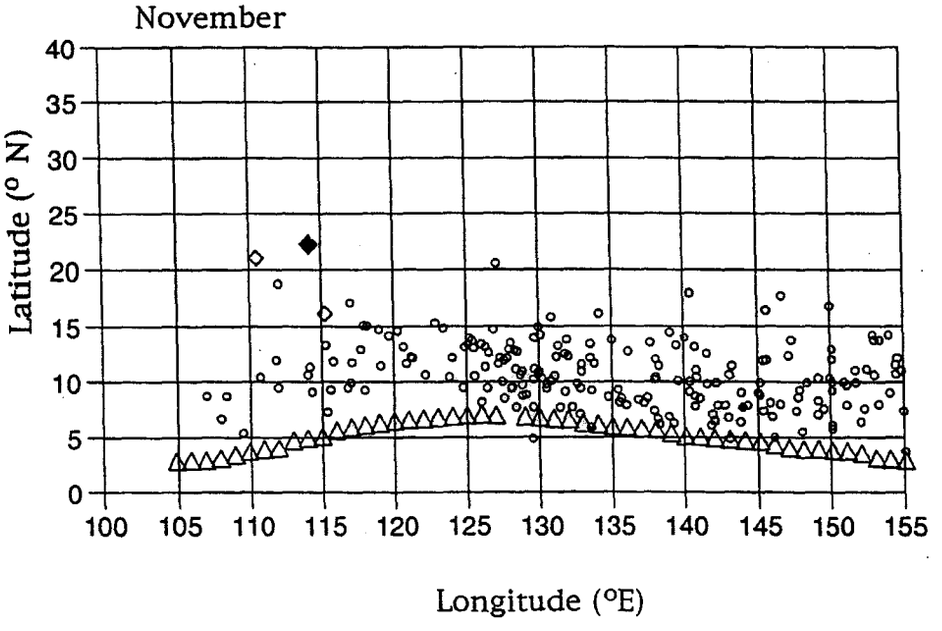

As shown in the diagrams, nearly all of the typhoons roughly are encircled by the larger values of vertical wind shear, indicting that a smaller value of vertical shear is the catalyst in the formation of typhoon. Furthermore, typhoons in the tropics can form without the assistance of the TUTT. The TUTT can be important in the high Southern Oscillation Index (SOI) years when the SSTs in the Eastern and central North Pacific are lower than normal and typhoons are found to form in association with TUTT cells in an area north of 20° N and 160° E (Lander, 1994). Some of these typhoons (*see* JTWC, 1989, 1992) that originate from cloud clusters near or beneath TUTT cells have these features: small-size storms, embedded in the easterly flow on the southwestern flank of a large subtropical high pressure system, and immersed in a relatively cloud-free environment.

In the early and middle typhoon season, tropical cyclones form within a belt of 15-20 degrees in association with the mean surface monsoon trough. However, a larger percentage is located on the northern side of the mean surface monsoon trough.

In the late typhoon season, when the mean surface monsoon trough recedes towards the equator, almost all the typhoons form on the northern side of the mean surface monsoon trough. It is because the values of vertical wind shear are larger and the planetary vorticity is lower on the south side of the surface monsoon trough. Typhoons that affect Hong Kong tend to originate in two regions. The first is within a belt of 10 degrees centered over the mean surface monsoon trough. During the peak season in August, a second region is located over the South China Sea (near 15°N and 115°E) because of warmer SST and smaller values of vertical wind shear in the interior of South China Sea. The typhoons that form outside these two regions and in association with TUTT cells are unlikely to affect Hong Kong.

Typhoon Intensity Changes

The changes in the typhoon intensity in the western North Pacific and South China Sea are shown in Figures 6 to 10. From these figures, some insight into the intensity changes that affect Hong Kong and coastal areas are obtained. Before presenting the discussion in the intensity changes, a brief outline of methodology in the analysis is given here.

The study area is divided into three regions: (1) the Philippine Islands, (2) Bashi-Balintang Channel, and (3) the South China Sea. In region (1), the Philippine Islands are divided into Luzon Island and the central Philippines (around 14.5 °N) where the tropical cyclones move along the southeast-northwestern direction. In terms of typhoon intensity, the tropical cyclones in regions (1) and (2) are divided into two groups: weak cyclones (less than 60 kts) and strong cyclones (greater than 60 kts).

In regions (1) and (2), the arrival time in each upstream track is determined when the tropical cyclones begin to cross the Philippine Islands or Bashi-Balintang Channel. Similarly, the departure time in the downstream track is determined when the tropical cyclones emerge from the Philippine Islands or Bashi-Balintang Channel. Both the arrival and the departure times are taken as zero at which all of the upstream and downstream tracks are aligned with these two time frames of reference. From the new adjusted time series, the mean, maximum, and minimum typhoon intensities are calculated at 6 hour intervals.

In region (3), a zero time reference is marked when the storm is found in the closest proximity of Hong Kong from each track. All tracks are aligned with this zero time of reference such that the calculations of the mean intensity similar to those in regions (1) and (2) are repeated. To determine the stage of the storm at which the tropical cyclones come to the closest proximity of Hong Kong Observatory, a symbol circle is used to indicate that the cyclone could pose the most threat to Hong Kong after entering the South China Sea.

Finally, to facilitate the discussion, tropical cyclone is used as the generic term. When the discussion involves the storm intensity, the technical terms are used in association with the intensity classification of the storm.

Figure 6. Changes of mean typhoon intensity (kts) passing over Luzon Island and central Philippines. Along the southeast-northwestern track: (a) strong storms (greater than 60 kts), (b) weak storms (less than 60 kts), and (c) weak storms (less than 60 kts). Dashed lines are the maximum and minimum wind intensity. Symbol circles refer to the time when the storms are in the closest proximity of Hong Kong.

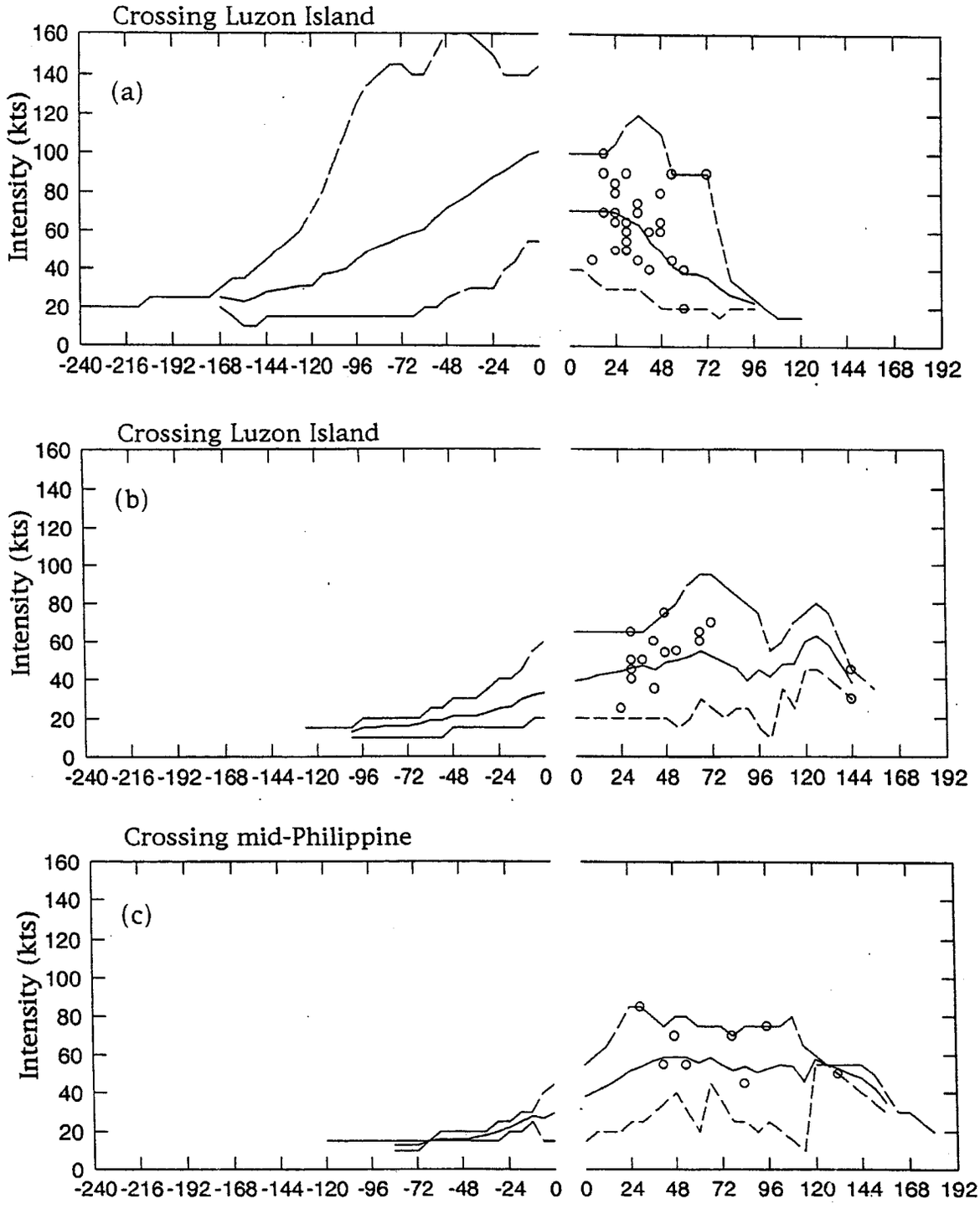

Figure 7. Changes of mean typhoon intensity (kts) crossing the Bashi-Balintang Channel. Along the southeast-northwestern track: (a) strong storms (greater than 60 kts), (b) weak storms (less than 60 kts). Along the east-west track : (c) strong storms (greater than 60 kts). Dashed lines are the maximum and minimum wind intensity. Symbol circles refer to the time when the storms are in the closest proximity of Hong Kong.

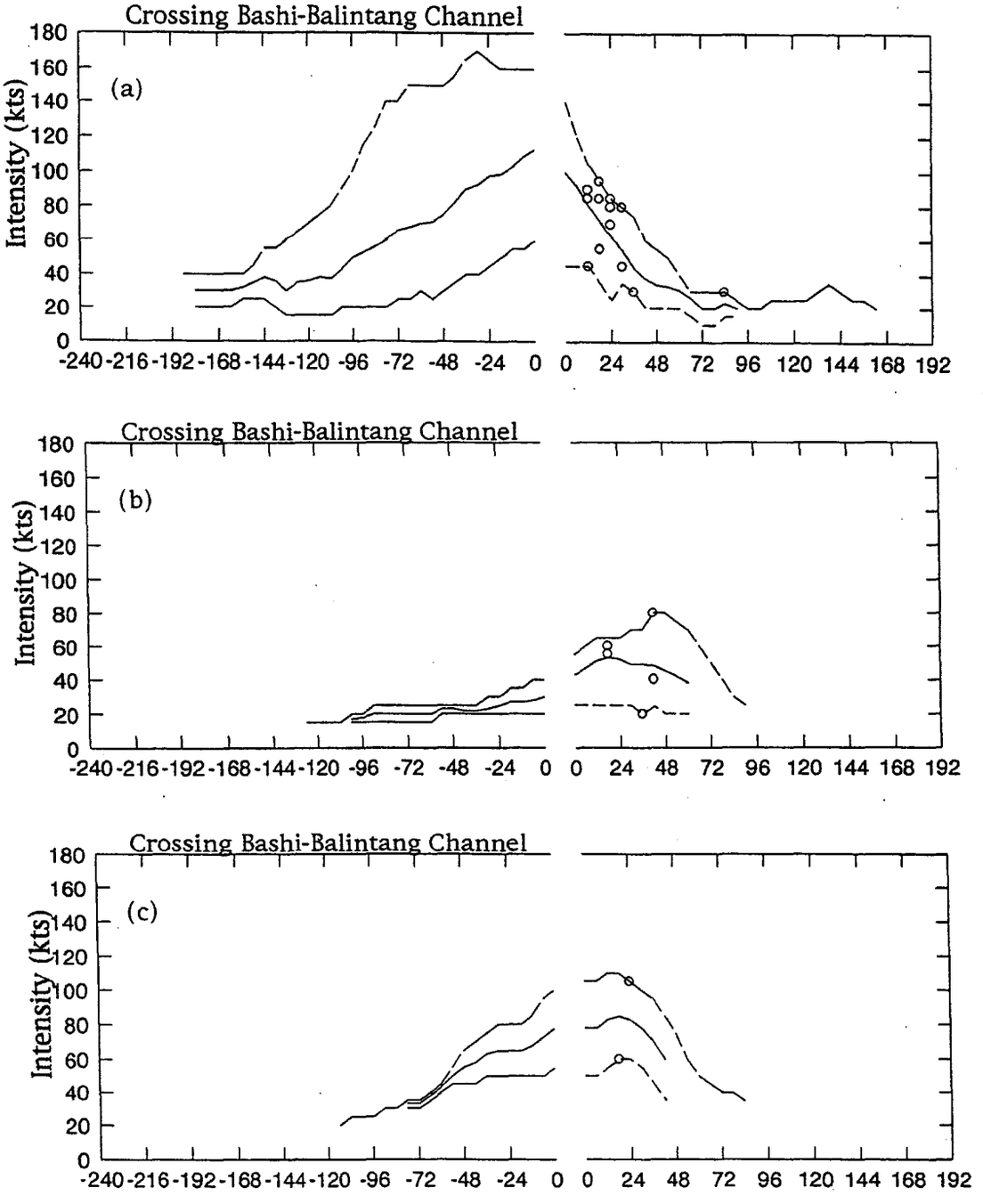

Figure 8. Changes of mean typhoon intensity (kts) for the storms that initially cross the Bashi-Balintang Channel in the east-west direction but re-curve later: (a) northeastern track, (b) southwestern track. Dashed lines are the maximum and minimum wind intensity. Symbol circles refer to the time when the storms are in the closest proximity of Hong Kong.

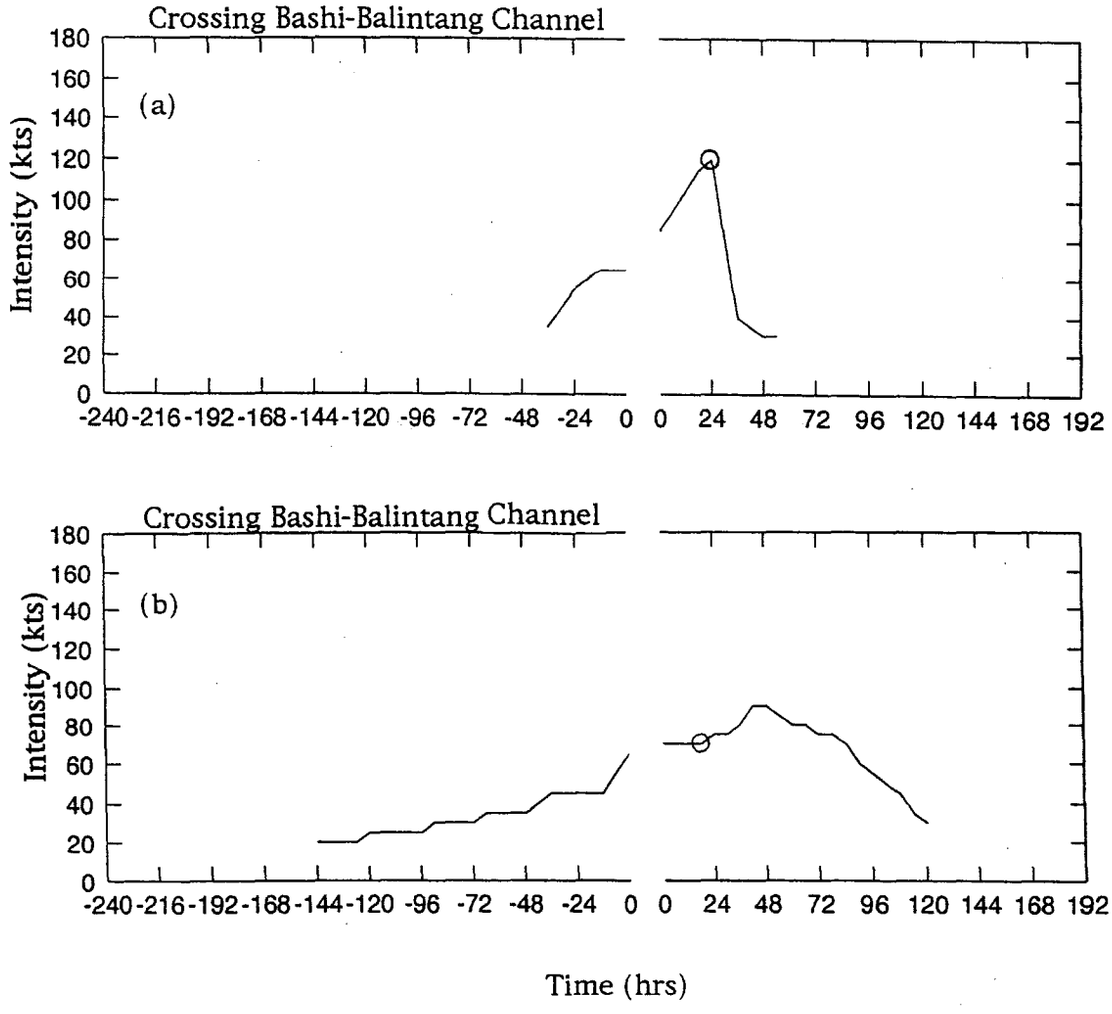

Useful Guidance for Forecasters

a. Points of origin of typhoons

During the typhoon season, the first step is to locate the surface monsoon trough on the daily surface map. In particular, a monitoring period begins when the position of the surface monsoon trough is found near the monthly mean position for a particular month. Special attention will be focused on the tropical cyclones, which form within a 5-degree belt centered over the surface monsoon trough.

b. Intensity changes

i. Strong storms (greater than 60 kts)

If the mean wind intensity exceeds 60 kts, Luzon and the Bashi-Balintang Channel along the eastern and northeastern rim of the South China Sea act like a "speed bump" to the roaring typhoons before they enter the South China Sea. The cool SST and larger values of vertical shear in the South China Sea act like a braking system. The South China Sea acts like a landing strip before the typhoons make landfall if they do not re-curve away from Hong Kong.

*Bashi-Balintang Channel

After sweeping through the Bashi-Balintang Channel, the intensity of tropical storms is lowered by 10 percent (from 110 to 100 kts). Within 48 hrs after the crossing, the mean intensity drops another 40 percent. The typhoons come to the closest proximity of Hong Kong within 24-48 hours with the majority of 69 percent within 24 hours.

*Luzon Island

When the typhoons emerge from Luzon Island, the mean intensity is reduced by 30 percent (from 100 to 70 kts). Having entered the South China Sea, the mean intensity is lowered by 60 percent within 48 hours after the crossing of Luzon. The typhoons penetrate to the closest proximity of Hong Kong within 24 hours with a majority (72 percent) within 24-48 hours. Note that the mean intensity of the storms does not drop as fast as those storms passing over Bashi-Balintang Channel.

ii. Weak storms (less than 60 kts)

If the mean wind intensity is less than 60 kts, Luzon Island and the Bashi-Balintang Channel do not appear to reduce the storm intensity.

*Bashi-Balintang Channel

After passing through the Bashi-Balintang Channel, the mean intensity of storms continue to increase from 30 kts to 50 kts (a 66 percent increase) in 24 hours. The storms are located in the closest proximity of Hong Kong within 24-48 hours. Note that one storm evolves successfully into a typhoon.

*Luzon Island

The mean intensity of the storms increases slightly from 30 kts to 40 kts after crossing over Luzon Island and finally up to 60 kts in 72 hours. About 25 percent of the storms will become typhoon and 75 percent of the storms will become severe tropical storms. The storms will enter the closest proximity of Hong Kong within 24 hours with the majority (81 percent) in 24-72 hours.

iii. Storms crossing over Central Philippines

When the storms move across the central Philippines, the mixed underlying surfaces of island and sea do not lower the intensity of the storm. In contrast, the mean intensity increases slightly by 10 percent (from 30 kts to 40 kts) after the crossing, and it reaches a maximum of 60 kts in 48 hours. About 50 percent of the storms become typhoons. Because the storms travel a longer distance, the length of time that the tropical cyclone takes to reach the closest proximity to Hong Kong ranges from 24 to 96 hours.

iv. Storms passing through the Bashi-Balintang Channel

If the storms enter the South China Sea from the east through the Bashi-Balintang Channel, the storms will be strengthened by 10 percent after traversing the Bashi-Balintang Channel. However, the storms will decay during the 24 to 72 hour period after sweeping through the Bashi-Balintang Channel if they maintain a latitudinal track.

v. South China Sea

If the storms form over or near 15 °N and 115 °E in the South China Sea, the storms could take some erratic tracks. The mean directions are: south-north direction, south-northeast direction, south-northwest direction, and roughly east-west direction.

Note that the intensity changes appear to undergo two periods of intensification in the south-northeast direction, south-northwest direction, and roughly east-west direction. Actually, the tropical cyclones occasionally travel along the erratic tracks such as looping, oscillatory or a trochoidal track. Therefore, Hong Kong may experience periods of intense tropical storm winds. Readers are referred to a reviewed paper on the occurrence of oscillatory and trochoidal tracks (Wang *et al.*, 1998).

Figure 9. **Changes of mean typhoon intensity (kts) for the typhoons originating in the South China Sea: (a) South-northwestern track. (b) South-northern track. Dashed lines are the maximum and minimum wind intensity. Symbol circles refer to the time when the storms are in the closest proximity of Hong Kong.**

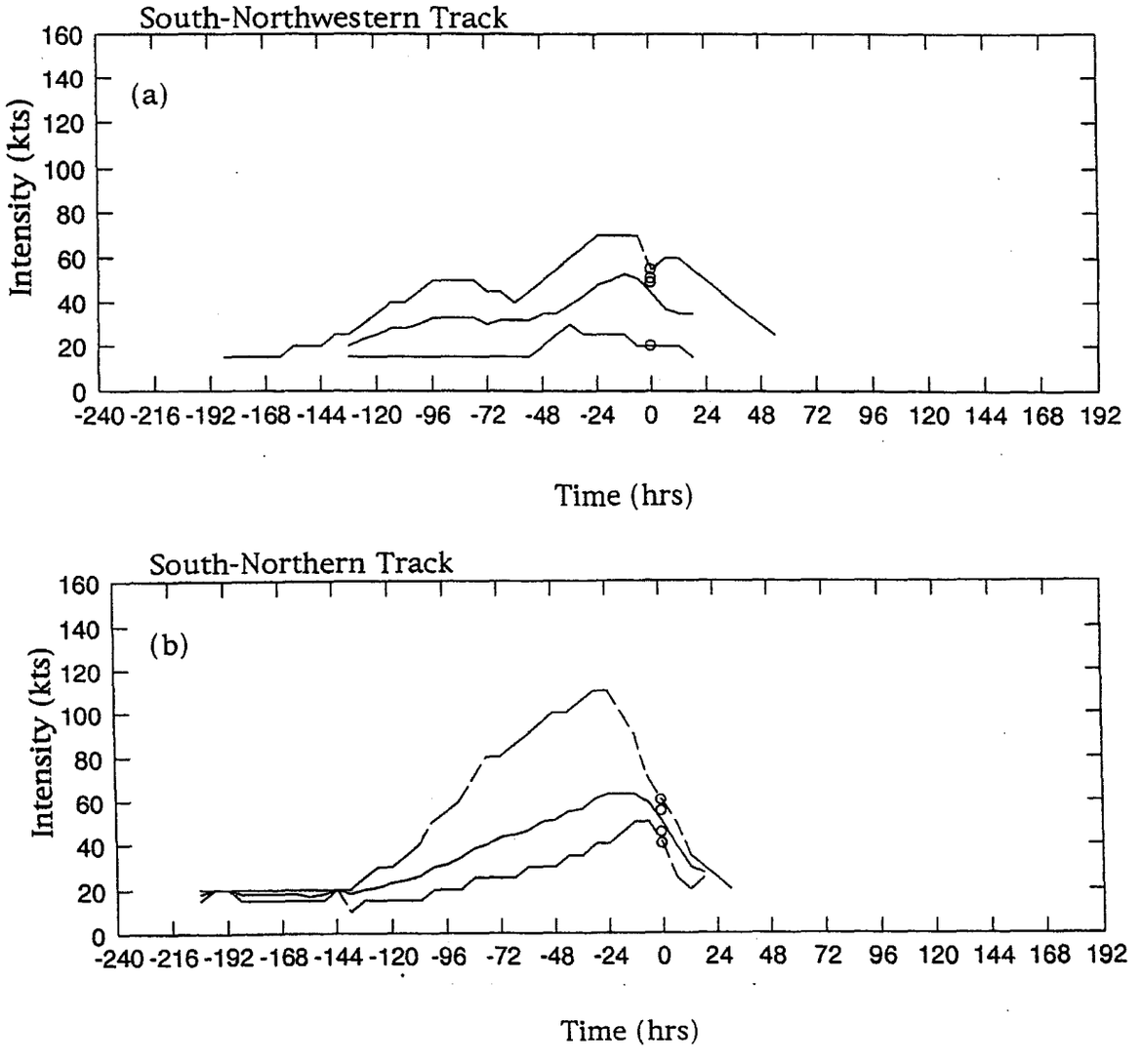

*South-Northwest Direction

If the storms move in a south-northwest direction (Figure 9a), the change in the typhoon intensity over 48 hours in the vicinity of Hong Kong is similar to those storms which move along the south-north direction. While these storms could achieve wind speeds of at least 60 kts in the proximity of Hong Kong, such intensity is relatively short-lived because the storms begin to fill as they make landfall over the coastal areas to the west of Hong Kong.

Figure 9. Changes of mean typhoon intensity (kts) for the typhoons originating in the South China Sea: (c) South-northeastern track (d) East-western track. Dashed lines are the maximum and minimum wind intensity. Symbol circles refer to the time when the storms are in the closest proximity of Hong Kong.

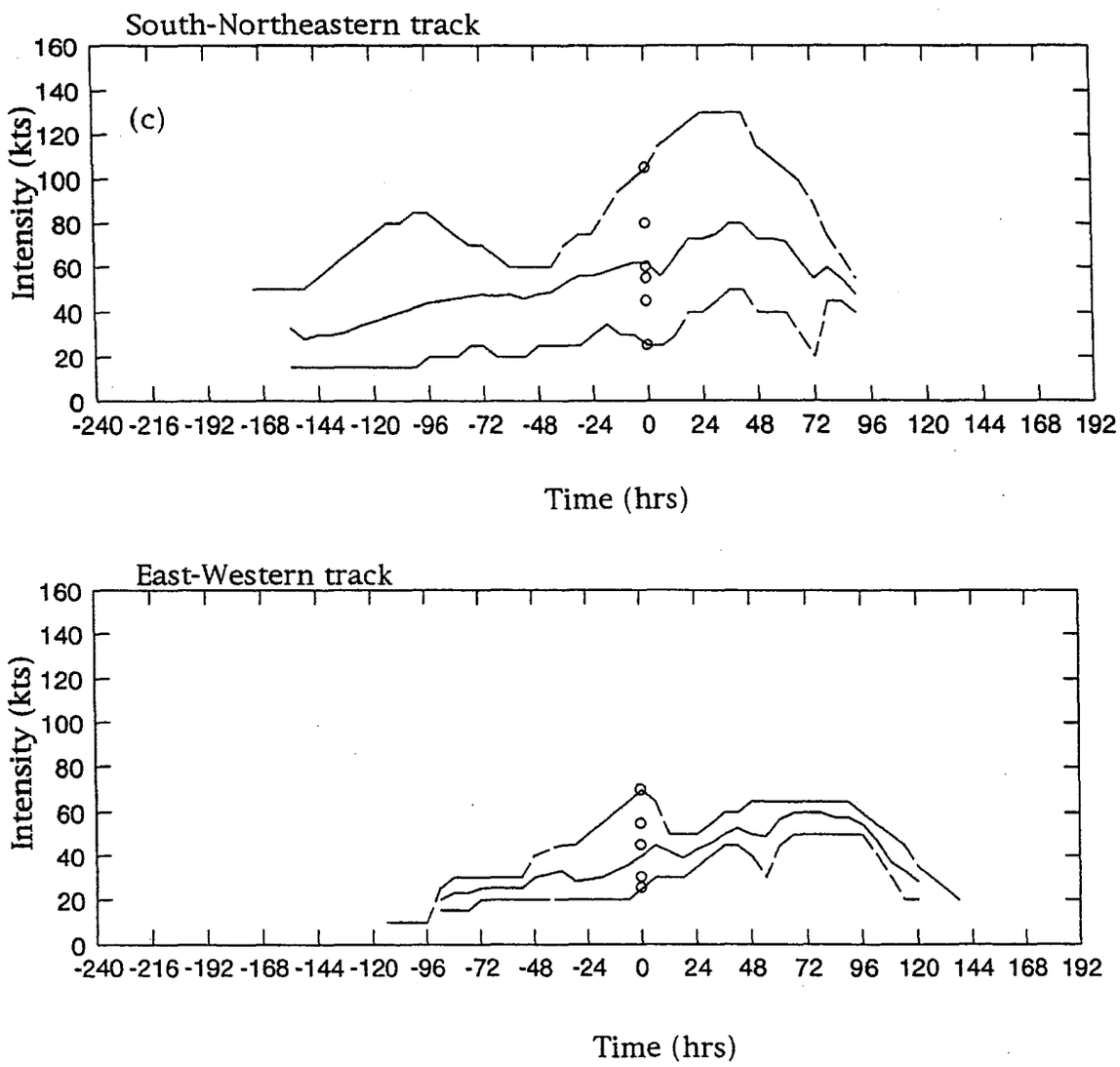

*South-North Direction

When the storms follow a south-north direction (Figure 9b), the storms continue to develop and reach a mean peak intensity of 60 kts when approximately about 24 hr offshore from Hong Kong. As the severe tropical storms or typhoons come even closer to Hong Kong, the outer flank of the storms feels the effect of the land mass and the storms begin to fill. The storms fill rapidly as they make landfall.

*South-Northeast Direction

When the storms move in the south-northeast direction (Figure 9c), they move roughly parallel to the coastline of the South China. The storms have a longer life span over the ocean without making immediate landfall. Therefore the storms can develop according to one of three scenarios: making landfall east of Hong Kong at a higher latitude, becoming mid-latitude cyclone, or dissipating over cooler water at a higher latitude. Under this situation, the winds of severe tropical storms or typhoons over Hong Kong can last up to 48 hours.

*East-West Direction

In the east-west direction (Figure 9d), the life span of the storm is relatively long (8-9 days). Despite their relatively long-lived nature, the storm intensity does not exceed the winds of severe tropical storms.

vi. Vertical wind shear

One must recognize that this climatological guidance is not a substitute for the daily operational analysis but only provides a reasonable basis for the first estimate, which can then be adjusted according to a given environment. Therefore, during a period when storms move towards South China Sea, the forecaster should daily examine the vertical wind shear since strong wind directional shear tends to prohibit a storm from intensification. If the vertical soundings are not available, one may analyze the 200 hPa height field. In the rapidly intensifying cases in the North Atlantic, the storms are on the edge of an upper-level cyclonic feature but never move directly under them.

Discussion

Not all tropical cyclones lose their intensity after they enter the South China Sea even though they may encounter strong vertical directional shear and relatively cooler SSTs. When the mean intensity is less than 60 kts, the intensity of storms continues to strengthen after passing over Luzon Island and the cooler seawater in the Bashi-Balintang Channel. This phenomena was also noted by Brand and Blelloch (1973) when they plotted the average intensity of a storm approaching the island against the changes in the storm intensity after crossing the Philippine Islands.

The occurrence of storms with intensity above or below 60 kts does not have a seasonal bias but is more dependent on the origin of the storms and the environmental conditions prior to entering the South China Sea. While the SST in the South China Sea is 1-2 degrees cooler than that in the western North Pacific Ocean, the monthly mean SST in the South China Sea during summer is still above 28° C. Therefore, additional mechanisms in the South China Sea probably influence the conditions of the storm environment, making it favorable for either intensification or dissipation.

a. Mixing through entrainment

The entrainment rate beneath the thermocline is directly proportional to the wind speed. One can estimate the entrainment rate, W_e, by $1.25 * \tau^{1.5}$ where τ is the wind stress with a value equal to $1.275 * 10^{-3} * C_d * U * U$. Here U is the wind speed and C_d is the drag coefficient given by $(0.73 + 0.069 * U)*10^{-3}$.

Figure 11 is a plot of the entrainment rates under various values of tropical cyclone wind force. When the tropical wind force is less than 30 m s^{-1} (60 kts), the entrainment rate does not change much and remains less than 0.05 cm s^{-1}. In contrast, when the tropical cyclone wind force exceeds 30 m s^{-1}, the entrainment rate increases rapidly with the increased wind speed. From the diagram, one can utilize the entrainment rate and determine which storm scale can generate a big enough entrainment rate such that the mixing of cooler water beneath the thermocline with the surface water can bring an negative effect on the intensity of the storm. This is feasible because the intensity of the storm will determine the length of time required to mix the cooler water beneath the thermocline with the warmer surface water.

Figure 11. **Entrainment rates in cm s^{-1} at various wind speeds. Symbol circles refer to the tropical depression. Symbol inverted triangles indicate the tropical storm. Symbol diamonds mark the severe tropical storm. Symbol dark circles represent typhoon. Triangles refer to the super typhoon.**

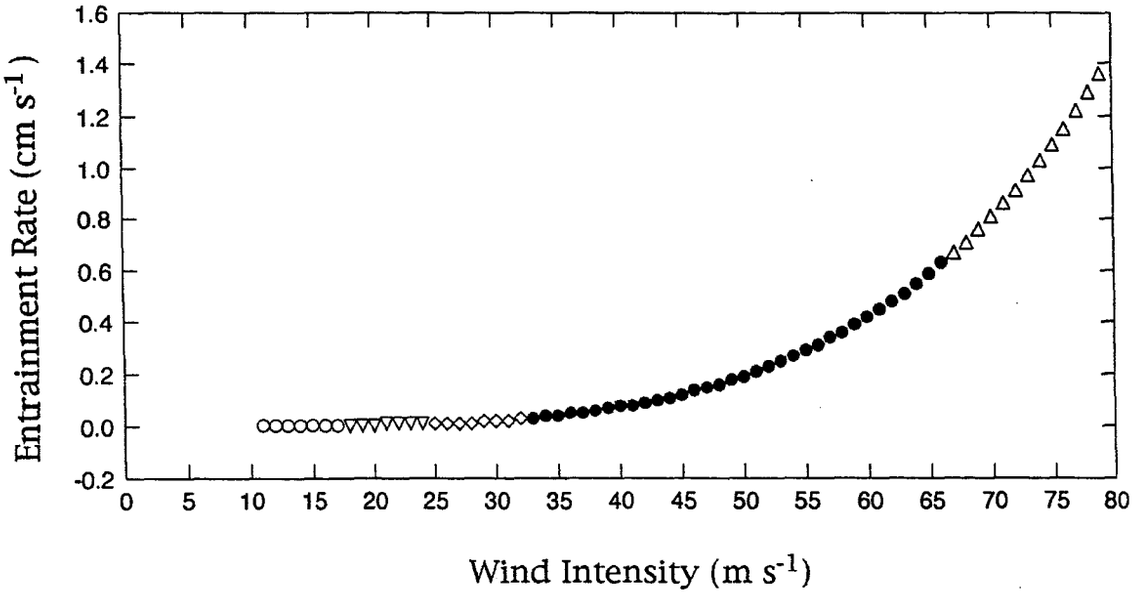

For instance, a severe tropical storm (30 m s^{-1}) will induce an entrainment rate of 0.02 cm s^{-1} (Figure 11). If the mean depth of the mixed layer is 50 m and ΔT ~ 10 °C across the thermocline in the North Pacific Ocean (Ando and McPhaden, 1997), the cooler water beneath the thermocline will reach the surface in about 69 hrs. If the storm moves at a mean speed of 6 m s^{-1}, the water column under a band of maximum surface wind (30 km) inside the storm will need about 1.4 hours to become well mixed. Similarly, if the mean depth of the mixed layer in the South China Sea is 20 m and ΔT ~8 °C across the thermocline (Wyrtki, 1961), the cooler water beneath the thermocline will reach the surface in about 27 hrs. In both cases, the entrainment rate is too weak under the band of maximum wind within a severe tropical storm to allow the water column to become well mixed. Therefore, the cooling in the SST under a severe tropical storm (less than 30 m s^{-1}) is not substantial.

Contrarily, a typhoon (with 60 m s^{-1}) will induce an entrainment rate of 0.42 cm s^{-1}. In the North Pacific Ocean, the cooler water beneath the thermocline will take about 3 hours to reach the sea surface. Similarly, in the South China Sea, the cooler water beneath the thermocline will take about 1.3 hours to replace the warmer water at the surface. If the typhoon moves at 6 m s^{-1} and the band of the maximum surface wind is 30 km, within 1.4 hours, the typhoon over the South China Sea can generate an entrainment of cooler water to mix with the mixed layer completely. However, under the same condition in the North Pacific Ocean, the mixing in the mixed layer is moderate.

Under similar synoptic conditions, a typhoon with a mean intensity exceeding 60 m s^{-1} can produce a negative feedback through air-ocean system and weaken the storm. For weaker storms (less than 60 kts), the storms are able to survive moving over island barrier and also a moderate negative feedback of air-ocean system.

b. Evaporative cooling of sea spray droplets

Lighthill *et al.* (1994) and Willoughby (1995) suggest that evaporative cooling of blowing sea spray at extreme wind speeds may inhibit storm intensification. This suggestion is supported by a numerical result that the intensity of a mature storm is slightly less than that of one without sea spray when the effect of sea sprays is included in a numerical simulation (Uang and Thorncroth, 1996). However, it is not completely determined at what wind speed the evaporative cooling begins to have a negative impact on the intensity of the storm.

Theoretical work postulates that breaking waves and sea spray would significantly affect air-sea heat and moisture exchange for wind speeds above 15 m s^{-1}. In a simulation of a tropical cyclone, the boundary layer evolves more realistically when the model included a generation function up to 24 m s^{-1} (Fairall *et al.*, 1994). In another numerical experiment, which includes consistent formulations of boundary layer parameterizations, the results indicate that the impact of sea spray on heat and moisture fluxes become important when the wind speed is above 25 m s^{-1} (Makin, 1998).

Direct measurements of sea spray droplets and turbulent fluxes above the wind speed of 25 m s^{-1} are not available. The observations of Humidity Exchanges Over the Sea Main Experiment (HEXMAX) program (DeCosmo *et al.*, 1996) showed that no significant variation for the humidity exchange coefficient with wind speed up to 18 m s^{-1} and for sensible heat exchange coefficient with wind speeds up to 23 m s^{-1}.

The key to modeling the effect of evaporation of sea spray droplets on heat and moisture transfer in the surface boundary layer is the generation function that produces sea spray droplets of various sizes. Andreas *et al.* (1995) have given a complete review on the accuracy of generation functions of various sea spray droplets. In addition to the review, Andreas (1998) also proposed a new sea spray generation for wind speeds up to 32 m s^{-1}. Two important conclusions are obtained from the review. The first is that the sea spray droplet production increases roughly as the third power of wind speed. This suggests that the evaporative cooling of sea spray droplets has a large impact on the sensible and moisture budgets in the surface layer under typhoon conditions. Second, higher temperature fosters larger spray moisture and latent heat fluxes because droplet temperature determines the rate at which spray droplets evaporate.

While there is great progress in our understanding of the role of sea spray in the heat and moisture transfer in the surface boundary layer, when the evaporative cooling of the sea spray droplets begins to have a negative feedback to the intensity of the storm is an active research area. Despite this, one must be aware that in a tropical cyclone, the majority of sea spray droplets evaporate in the droplet evaporation layer (0.1 m to less than 10 m). Subsequently, the layer is cooler and moister than the surface layer would be under the identical condition but without spray. How the transfer of heat and moisture from the surface boundary to the boundary layer aloft will affect the intensity of the tropical cyclone. In addition, the vertical heat flux is no longer constant with height because of the elevated sources and sinks for heat and moisture.

c. A challenge

While the mean intensity of a typhoon is diminished somewhat in many cases as compared to those in the open ocean, its gusty winds remain at typhoon wind force. Therefore, the "diminishing" typhoons can still bring destructive, gusty winds and excess rainfall to Hong Kong. In addition to know the intensity changes in the South China Sea, the forecasters need to understand how the typhoons interact with the complex terrain of Hong Kong and their effects on the distributions of local rainfall and winds as the typhoons either enter or pass near by. The interaction between the typhoon and Hong Kong complex terrain will be the theme in the Part 2 of this study.

References

Ando, K., and M.J. MCPhaden (1997) Variability of surface layer hydrography in the tropical Pacific Ocean. *J. Geophy. Res.*, 102, 23063-23078.

Andreas, E.L. (1998) A new sea spray generation function for wind speeds up to 32 m s^{-1}. *J. Phys. Oceanogr.*, 28, 2175-2184.

Andreas, E.L., J.B. Edson, E.C. Monahan, M.P. Roualt, and S.D. Smith, 1995: The spray contribution to net evaporation from the sea: a review of recent progress. *Bound-Layer Meteor.*, 72, 3-5.

AWS/USAF (1961) *The practical aspect of tropical meteorology.* C. S. RAMAGE (Ed.)., AWSM 105-48, Vol. II/AFCRC-TN-60-455.

Atkinson, G.D. (1970) *Gradient-level wind charts over the tropics.* Air Weather Service (USAF) Technical Rep. 215, Vol. II.

Baik, J.J., and J.S. Paek (1998) A climatology of sea surface temperature and the maximum intensity of western North Pacific tropical cyclones. *J. Meteor. Soc. Japan*, 76, 129-137.

Brand, S., and J.W. Blelloch (1973) Changes in the characteristics of typhoons crossing the Philippines. *J. Appl. Meteor.*,12, 104-109.

Brand, S., and J.W. Blelloch (1974) Changes in the characteristics of typhoons crossing the island of Taiwan. *Mon Wea. Rev*, 102, 708-713.

Breaker, L.C., L.D. Burroughs, Y.Y. Chao, J.F. Culp, N.L. Guinasso, R.L. Teboulle, and C.R. Wong (1994) The impact of hurricane Andrew on the near-surface marine environment in the Bahamas and the Gulf of Mexico. *Wea. Forecasting*, 9, 542-556.

Challa, M., R.L. Pfeffer, Q. Zhao, and S.W. Chang (1998) Can eddy fluxes serve as a catalyst for hurricanes and typhoon formation? *J. Atmos. Sci.*, 55, 2201-2119.

Chin, P.C. (1972) *Tropical cyclone climatology for the China Seas and western Pacific from 1884 to 1970, Vol. 1 : Basic data.* Royal Observatory Technical Memoir No. 11. Royal Observatory, Hong Kong.

Chin, P.C. (1958) *Tropical cyclones in the western Pacific and China Sea area 1884-1953.* Royal Observatory Technical Memoir No. 7. Royal Observatory, Hong Kong.

DeCosmo, J., and co-authors (1996) Air-sea exchange of water vapor and sensible heat: The Humidity Exchange Over the Sea (HEXOS) results. *J. Geophys. Res.*, 101, 12001-12016.

DeMaria, M. and J. Kaplan (1994) Sea surface temperature and the maximum intensity of Atlantic tropical cyclones. *J. Climate*, 7, 1324-1334.

DeMaria, M., J.J. Baik, and J. Kaplan (1993) Upper-level eddy angular momentum fluxes and tropical cyclone intensity change. *J. Atmos. Sci.*, 50, 1133-1147.

Dong, K. (1988) On the relationship between tropical cyclone motion and intensity. *Mon. Wea. Rev*, 116, 964-968.

Elsberry, R.L., G.J. Holland, H. Gerrish, M. DeMaria, C.P. Guard and K. Emanuel (1992) Is there any hope for tropical cyclone intensity prediction? - A panel discussion. *Bull. Amer. Meteor. Soc.*, 73, 264-275.

Emanuel, K.A. (1988) The maximum intensity of hurricanes. *J. Atmos. Sci.*, **45**, 1143-1155.

Erickson, C.O., and J.W. Winston (1972) Tropical storm, mid-latitude, cloud band connections and the autumnal build up of the planetary circulation. *J. Appl. Meteor.*, **11**, 23-26.

Evans, J.L. (1993) Sensitivity of tropical cyclone intensity to sea surface temperature. *J. Climate*, **6**, 1133-1140.

Fairall, C.W., J. D. Kepert and G.J. Holland (1994) The effect of sea spray on surface energy transports over the ocean. *Global Atmos. Ocean System*, **2**, 121-142.

Fedorov, K.N, and co-authors (1979) Thermal response of the ocean on the passage of hurricane Ella. *Oceanology Engl. Transl.*, **19**, 656-661.

Fok, L. (1997) *A survey on the tropical cyclones of the western North Pacific Ocean from 1966 to 1995: origin, dissipation, path, and frequency.* Department of Geography and Geology, University of Hong Kong, Hong Kong. 79 pp.

Gray, W. M. (1998) The formation of tropical cyclones. *Meteor. Atmos. Phys.*, **67**, 37-69.

Hsu, Y.C. (1960) *The problems of typhoon forecasting over Taiwan and its vicinity.* Proc. of the U. S. Asian Military Weather Symposium, Feb. 9-12, 1960.

JTWC (1992) *Synoptic discussion of Tropical Storm Helen.* 1992 Annual Tropical Cyclone Report. F. Wells, (Ed.), Joint Typhoon Warning Center, Guam.

JTWC (1989) *Synoptic discussion of Super Typhoon Gordon.* 1989 Annual Tropical Cyclone Report. F. Wells, (Ed.), Joint Typhoon Warning Center, Guam.

Jeary, A.P. (1997) The wind climate of Hong Kong. *J. Wind Eng. Ind. Aerodyn.*, **72**, 433-444.

Jordan, C.L., and N.L. Frank (1964) *On the influence of tropical cyclones on the sea surface temperature field.* Florida State University, Tallahassee, Florida, USA.

Kuroda, M., A. Harada and K. Tomine (1998) Some aspects on sensitivity of typhoon intensity to sea-surface temperature. *J. Meteor. Soc. Japan*, **76**,145-151.

Kyle, W.J. (1999) 1998 tropical cyclone summary for the western North Pacific Ocean (west of 180 degrees). *Bull. Hong Kong Meteoro. Soc.* **9**, 46-66.

Lander, M.A. (1994) An exploratory analysis of the relationship between tropical storm formation in the western North Pacific and ENSO. *Mon. Wea. Rev,* **122**, 636-651.

Lighthill, J., G. Holland, W. Gray, C. Landsea, G. Graig, J. Evans, Y. Kurihara and C. Guard (1994) Global climate change and tropical climate. *Bull. Amer. Meteor. Soc,* **75**, 2147-2157.

Makin, V.K. (1998) Air-sea exchange of heat in the presence of wind waves and spray. *J. Geophys. Res.*, **103**, 1137-1152.

Merrill, R.T. (1988) Environmental influences on hurricane intensification. *J. Atmos. Sci.*, **45**, 1678-1687.

Merrill, R.T. (1987) *An experiment in the statistical prediction of tropical cyclone intensity change.* NOAA Tech. Memo. NWS NHC 34, 33 pp.

Miller, B.I. (1958) On the maximum intensity of hurricanes. *J. Meteor.*,15, 184-195.

Molinari, J. and D. Vollaro (1989) External influences on hurricane intensity. Part I: Outflow layer eddy angular momentum fluxes. *J. Atmos. Sci.*, 46, 1093-1105.

Molinari, J. and D. Vollaro (1990) External influences on hurricane intensity. Part II: Vertical structure and response of the hurricane vortex. *J. Atmos. Sci.*, 47, 1902-1918.

Nyoumura, Y. and H. Yamashita (1984) On the central pressure change of tropical cyclones as a function of sea-surface temperature and land effect. *Geophy. Mag.*, 41, 45-59.

NOCC/JTWC (1991) *Tropical cyclones affecting Guam (1671-1990).* Tech Note 91-2. NOCC/JTWC, COMNAVMARIANAS, PSC 489, Box 12, FPO AP 96540-0051. 45 pp.

Ooyama, K.V. (1969) Numerical simulation of the life cycle of tropical cyclones. *J. Atmos. Sci.*, 26, 3-40.

Ooyama, K.V. (1982) Conceptual evolution of the theory and modeling of the tropical cyclone. *J. Meteor. Soc. Japan*, 60, 369-380.

Palmen, E. (1956) *Formation and development of tropical cyclones*. Proc. of the Tropical Cyclone Symposium, Brisbane, 213-231.

Pfeffer, R.L., and M. Challa (1981) A numerical study of the role of eddy fluxes of momentum in the development of Atlantic hurricanes. *J. Atmos. Sci.*, 38, 2393-2398.

Pun, K.S. (1966) A survey of the climatological phenomena of typhoons of western North Pacific Ocean and the South China Sea with special reference to Hong Kong. University of Hong Kong, Hong Kong.

Ramage, C.S. (1972) Interaction between tropical cyclones and the China Seas. *Weather*, 27, 484-494.
Ramage, C.S. (1974) The typhoons of October 1970 in the South China Sea: intensification, decay and ocean interaction. *J. Appl. Meteor.*, 13, 739-751.

Riehl, H. (1979) *Climate and Weather in the Tropics*. Academic Press, 465 pp.

Rogers, R.F. and R.E. Davis (1993) The effect of coastline curvature on the weakening of Atlantic tropical cyclones. *International J. Climatology*, 13, 287-299.

Sadler, J.C. (1975) *The upper tropospheric circulation over the global tropics*. Department of Meteorology, University of Hawaii. Rep. UHMET,75-05,35 pp.

Sadler, J.C. (1976) A role of the tropical upper tropospheric trough in early season typhoon development. *Mon. Wea. Rev.*, 104, 1266-1278.

Sadler, J.C. (1978) Mid-season typhoon development and intensity changes and the tropical upper tropospheric trough. *Mon. Wea. Rev.*, 106, 1137-1152.

Sadler, J.C. and B.E. Harris (1970) *The mean tropospheric circulation and cloudiness over southeast Asia and neighboring area.* Scientific Report No. 1, University of Hawaii.

Sakaida, F. (1998) Sea surface cooling caused by typhoons in the Tohoku area in August 1989. *J. Geophy. Res.*, 103, 1053-1065.

Sanford, T.B., P.G. Black, J.R. Haustein, J.W. Feeney, G.Z. Forristall, and J.F. Price (1987) Ocean response to a hurricane Part I: Observations. *J. Phys. Oceanogr.* 17, 2065-2083.

Shay, L.K., P.G. Black, A.J. Mariano, J.D. Hawkins and R.L. Elsberry (1992) Upper ocean response to hurricane Gilbert. *J. Geophy. Res.*, 97, 20227-20248.

Shoemaker, D.N. (1991) *Characteristics of tropical cyclones affecting the Philippine Islands*. Tech Note 91-1. NOCC/JTWC, COMNAVMARIANAS, PSC 489, Box 12, FPO AP 96540-0051. 35 pp.

Simpson, J., E. Ritchie, G.J. Holland, J. Halverson and S. Stewart (1997) Mesoscale interaction in tropical cyclone genesis. *Mon. Wea. Rev.*, **125**, 2643-2661.

Stramma, L., P. Cornillon and J.F. Price (1986) Satellite observations of sea surface cooling by hurricanes. *J. Geophy. Res.*, **91**, 5031-5035.

Tsui, K.S., G.J. Bell and P.C.W. Fung (1977) Change in intensity of typhoons which develop cloud-plume outflow aloft. *Quart. J. Roy. Meteor. Soc.*, **103**, 151-156.

Tuleya, R.E. (1994) Tropical storm development and decay: sensitivity to surface boundary conditions. *Mon. Wea. Rev*, **122**, 291-304.

Uang, C.L. and C. Thorncroft (1996) *Evolution of tropical cyclone boundary layer.* 7th Conf. Mesoscale Processes. Reading, U.K., Amer. Meteor. Soc., 183-185.

Wang, B., R.L. Elsberry, Y. Wang and L. Wu (1998) Dynamics in tropical cyclone motion: a review. *Chinese J. Atmos. Sci.*,**22**,416-434.

Willoughby, H.E. (1995) Mature structure and evolution. *Global Perspectives On Tropical Cyclones*. R. L. Elsberry, (Ed.)., WMO/TD NO. 693.21-62.

Wong, N.Y. (1979) *Sea surface temperature in the South China Sea.* Royal Observatory Technical Note No. 61. Royal Observatory, Hong Kong. 70 pp.

Wu, C.C. and H.J. Cheng (1999) An observational study of environmental influences on the intensity changes of typhoons Flo (1990) and Gene (1990). *Mon. Wea. Rev*, **127**, 3003-3031.

Wyrtki, K. (1961) *Physical Oceanography of the Southeast Asia Waters*. Scripps Institute of Oceanography, University of California. 195 pp.

Yim, W.W.S. (1996) Vulnerability and adaptation of Hong Kong to hazards under climatic change conditions. *Water, Air, and Soil Pollution.* **92**, 181-190.

Zehr, R.M. (1992) *Tropical Cyclongenesis in the western North Pacific.* NOAA Technical Report NESDIS 61, RAMM Branch, Colorado State University. 181 pp.

M.R. Peart [1], W.J. Kyle [1] and R.D. Hill [2]

[1] Department of Geography, The University of Hong Kong, Pokfulam Road, Hong Kong
[2] Department of Ecology and Biodiversityy, The University of Hong Kong, Pokfulam Road, Hong Kong

Extracting Water from Clouds in Hong Kong

Abstract

The direct interception and extraction of wind-driven water droplets in fog and clouds by various types of vegetation has been chronicled in the literature for many areas and may play an important role in maintaining moisture supply to vegetation. In Hong Kong no literature exists on this phenomenon although observations in upland areas suggests that vegetation is capable of extracting moisture from wind-blown clouds passing through it. This study reports on a preliminary attempt to test the feasibility of extracting water from clouds passing over upland areas and to gain some insight into the factors relevant to the process. An instrument, termed a neblinometro was designed and constructed for this purpose and exposed near the summit of Tai Mo Shan, the highest peak in Hong Kong. Preliminary results show that such an instrument is capable of extracting considerable amounts of water from clouds, particularly in the spring months. Results also suggest that collection efficiencies are largely determined by the interplay of collection screen configuration, the droplet size distributions in clouds and the air flow patterns relative to the site of the neblinometro.

Introduction

The deposition of the airborne water droplets in fog and cloud onto vegetation to yield larger water drops which can then fall to the ground as fog drip is now a well-documented hydrological process. In some ways it is similar to the interception of rainfall by vegetation. However, whereas interception and re-evaporation of rainfall represents a loss of the effective precipitation input to a catchment, fog drip represents a potential gain. Fog drip arises as fog or cloud blows through a forest canopy and collects on the leaves. Drops form, and some of these drip to the ground forming a supplement to the rainfall reaching the ground under the forest canopy.

The liquid water content of a cloud, even if no precipitation is present, may range up to 1 gram per cubic metre. Although this figure seems low at first sight, it must be realized that even with light winds of the order of 3-5 metres per second, cloud-air passes through a vertical area of one square metre at an approximate rate of 10,000 to 18,000 cubic metres per hour. Hence, if this water could be extracted completely, up to 10-18 litres of water per square metre per hour would be yielded.

Investigations of cloud water have mainly focused upon three aspects: the chemistry of the water (e.g Lovett *et al.*,1982 Falconer and Falconer, 1980, Chandler *et al.*, 1988); the ecological role of the water as examined in the reviews of Kerfoot (1968) and Stadtmuller (1987) and the work of Cavelier and Mejia (1990) and finally the

implications of the water in terms of resource and land use potential (*e.g.* Cereceda *et al.*, 1992, Schemenauer 1988, and Schemenauer and Cereceda 1991) and streamflow (*e.g.* Gurnell, 1976). These categories are, of course, not mutually exclusive. For example, the chemistry may affect plant development and growth (*e.g.* Gindel 1966) while Lovett *et al.* (1992) recognize that cloud droplet deposition may provide both beneficial and harmful substances to plants. Hutley *et al.* (1997) emphasize the crucial role of cloud and fog as water sources in some Australian forests. The water quality also governs its suitability as a water supply (*e.g.* Cereceda *et al.*, 1992 and Schemenauer and Cereceda 1992).

In a review of mist precipitation on vegetation Kerfoot (1968) provides evidence of some very early qualitative observations on the phenomenon such as those of Glas (1764) in the Canary Islands and White's (1789) observations in Berkshire, England. The first examples of detailed discussion on the relationship between fog distribution and plants can be found in work on the coastal redwoods in California. For example, Kerfoot (1968) cites Cannon (1901), Cooper (1917) and Phillips (1926). Cloud water investigations therefore have a long history.

Studies of cloud and fog water interception have a wide spatial coverage as evidenced by the papers of Schemenauer and Cereceda (1992), Ekern (1964) and Juvik and Perreira (1974). However, cloud water has received little attention in the Asian region. For example, Schemenauer and Cereceda (1991) when referring to Asia state:

> "This vast continent with major desert regions, including some bordering coastlines, has almost no reported observations of fog-water collection by vegetation and no concerted efforts to work with fog collectors. The exceptions are some discussions of fog covered hills in the rainy climates of Southeast Asia ... .."

In a review of cloud forests in the Humid Tropics Stadtmuller (1987) with reference to Asia and in terms of specific areas cites works on Malaysia, New Guinea and the Himalayas.

In Hong Kong for the period 1961-1990 the months of February to June inclusive have average percent cloud cover in excess of 70 percent and mean relative humidities in excess of 80 percent which may be indicative of the possibility of the existence of cloud water. Further support for this is provided by Chin (1986) who reports that in Spring widespread fog or low stratus cloud which is often persistent may form.

Given the existence of cheap potable water from China, cloud water has no role to play in water supply in Hong Kong. However, investigating cloud water in Hong Kong is attractive on two counts. The chemistry of the air, given the generally southerly wind direction associated with low cloud and mist development in the Spring should reflect oceanic influences and would afford an interesting and useful contrast to conditions which prevail at other times of the year. For example, the surge of the winter monsoon may generate rainfall with origins over China and this may contain pollutants from Guangdong Province. However, problems with keeping the sampler clean and therefore the possibility of contamination of samples precluded expansion of the study to include this topic.

Cloud water may, in Hong Kong, provide an input of water to plants at a time when they may be suffering from physiological drought. It is this aspect which may be useful in the Hong Kong Special Administrative Region (HKSAR). In Hong Kong for the period 1961-90 91percent of the rainfall recorded at the Observatory fell in the period from April to October inclusive. Jackson and Hsu (1992) report that this is similar to that reported by Starbuck (1950) and they also note that Cheng (1978) reports 85 percent of rainfall occurring in the period May to September. This may be indicative of water shortage for human consumption and plants during the months of October to April. However, account must be taken of water stored in the soil. Jackson and Hsu (1992) have calculated monthly water deficits for plant growth in Hong Kong using a number of models and assumptions. They report that "under most assumptions, the period of limited or no deficit is very substantial, from April to at least October or November". This largely agrees with the rainfall input. They do, however, go on to state that for some

models noticeable deficits are confined to December and January but caution that with low soil storage capacities there can be a very long dry period. Evidence of physiological stress on hillslopes in Hong Kong is provided by the browning of the grasses and ferns during the winter dry period.

Figure 1. **Soil Moisture Suction measured at Kadoorie Agricultural Research Centre (KARC) from July, 1989 to May, 1990 inclusive (*unpublished data from* Peart)**

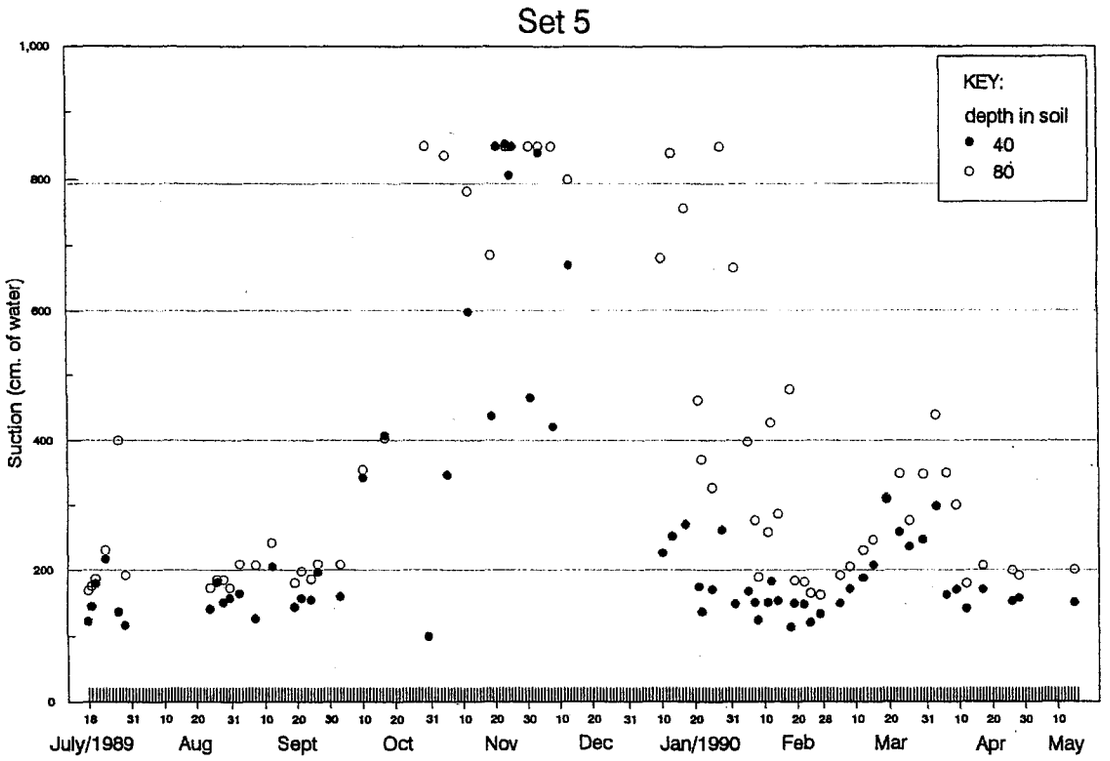

Quantitative data on seasonal variation of soil moisture in Hong Kong are provided by the soil moisture tensiometer data presented in Figure 1 which plots the suction force with which water is held in the soil. As the water content of the soil decreases due to evaporation and transpiration the force with which the remaining water is held by the soil particles rises. Consequently, the greater the suction the lower soil moisture. Data is presented for two depths within the soil layers 40 and 80 cm. The data evidences a spell of very high suction in November 1989 and a secondary peak in April 1990, while in the wet season of 1990 suction declines to much lower levels. These field observations, made on a hillslope at the Kadoorie Agricultural Research Centre and above 200 m PD, support the possibility of lower water availability in the soil during the dry season.

Given the possibility of a water deficit in the soil during the period when meteorological conditions may permit the occurrence of cloudwater, assessment of the potential of cloudwater is of some interest to Hong Kong. The following text examines the feasibility of extraction of cloud water at a high altitude site in Hong Kong including instrument design.

Study Area

The HKSAR is situated on the South China coast and lies less than 200 km south of the Tropic of Cancer (Figure 2). Structually the HKSAR is part of South East China and lies on the SE margin of the Cathaysia Block (Fletcher *et al.*, 1997). Essentially the HKSAR is an archipelago since only the New Territories and the

Figure 2. The Hong Kong Special Administrative Region of China
(*after* Survey & Mapping Office, Lands Department, HKSAR, 2000)

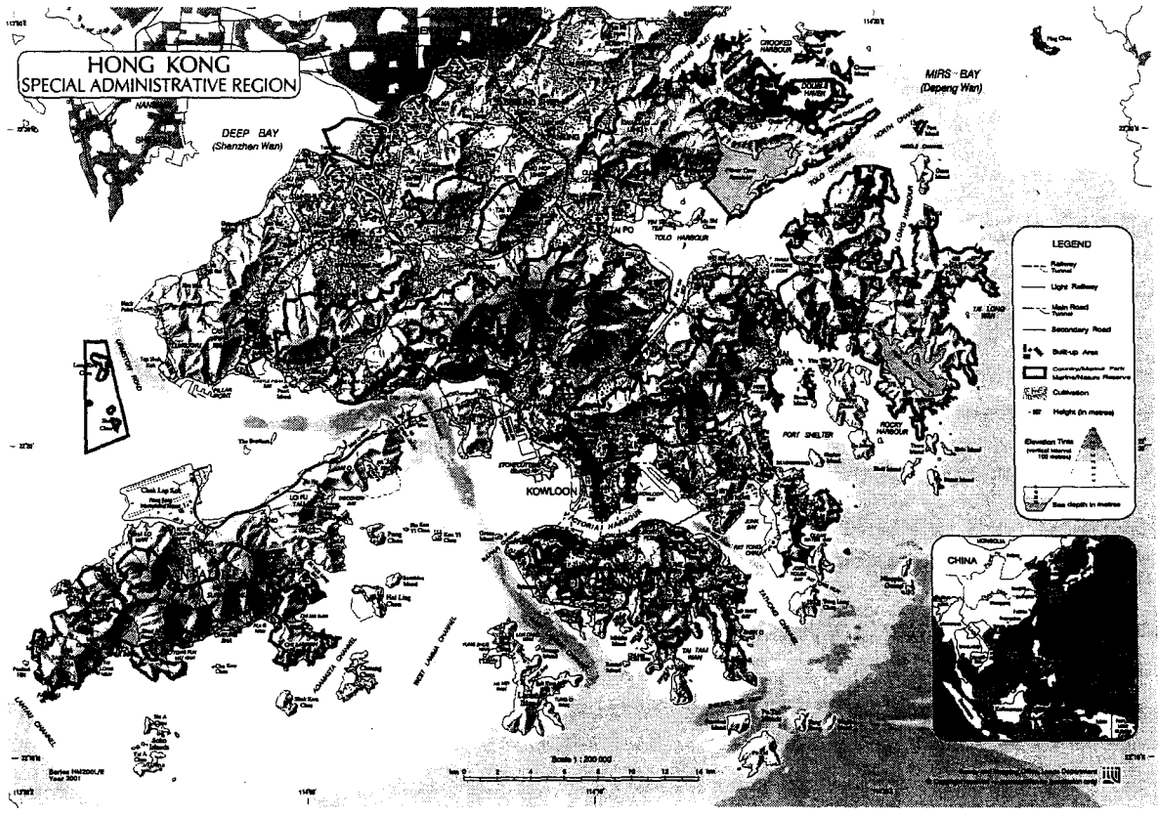

Kowloon Peninsula physically join the mainland (Figure 2). The remainder of the HKSAR consists of two large islands, Lantau 142 km² and Hong Kong Island 78 km², along with well over 200 other smaller islands. The climate, topography and vegetation of Hong Kong SAR and the study site will briefly be described.

i) CLIMATE

Based upon the regional classification of China proposed by Huang Bing-wei (1959) the HKSAR lies within the southern humid subtropical belt. This climate zone is characterized by mild winter temperatures and hot and humid summers, the latter being characterized both by sultriness and rainfall, over 80 percent of which occurs during the period from May to September (Chin, 1986). Fog or mist may sometimes occur in December, January and February (Chin, 1986). In March, Chin (1986) reports that, due to an increase in temperature and humidity, fog and mist become prevalent. Bright sunshine is at a minimum during this month. Chin (1986) also notes that during spring fog or very low stratus cloud may form and this may be persistent. Their formation may relate to the incursion of warm southerly winds.

Information on cloud cover at Sek Kong is provided in Figure 3. Annual cloud cover data indicates the potential for cloud water with, for example, a cloud cover of 7/8 or 8/8 occurring some 40 percent of the time.

Figure 3. Annual Cloud Cover Frequency Distribution at Sek Kong Airfield (SEK) derived from data from October, 1983 to June, 1991 inclusive held at Hong Kong Observatory (*unpublished data from* Kyle)

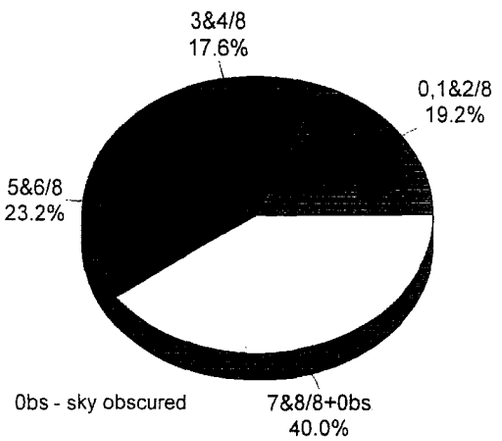

ii) TOPOGRAPHY

As noted by Styles and Hansen (1989) physiographically the HKSAR is an extension of the South China coastal massif. Moreover, despite its limited area (1094 km²) it exhibits marked spatial variations in relief and topography. Figure 4 presents a contour map showing some of the major hills and ranges in Hong Kong. Many of the upland hill masses are elongate in shape which according to Styles and Hansen (1989) evidence the northeast to southwest trend of the general topography. A subordinate northwest to southeast trend can also be seen in some areas (Styles and Hansen, 1989). Hong Kong has three peaks (Table 1) that are over 850 m in height. These are Tai Mo Shan (957 m PD) located in the central New Territories and Fung Wong Shan (Lantau Peak) and Tai Tung Shan (Sunset Peak), 934 and 869 m PD respectively, both of which are located on Lantau Island. Large areas of flatland are limited to the north-west and north, the Yuen Long, Kam Tin and Sheung Shui plains and only 12.4 percent of the HKSAR is above 300 m in elevation according to Styles and Hansen (1989).

Figure 4. 3-D Contour Map of HKSAR (*after* Styles and Hansen, 1989)

Table 1. Elevation of Twenty Highest Summits in HKSAR (*after* Styles and Hansen, 1989)

Name of Summit	Location	Height (m PD)
1. Tai Mo Shan	Central NT	957
2. Fung Wong Shan (Lantau Peak)	Lantau Island	934
3. Tai Tung Shan (Sunset Peak)	Lantau Island	869
4. Sheung Tung Au	Lantau Island	766
5. Nei Lak Shan (Ngong Ping)	Lantau Island	751
6. Ma On Shan	East Central NT	702
7. Ngau Ngak Shan (The Hunch Backs)	East Central NT	680
8. Tso Shan (Grassy Hill)	Central NT	645
9. Wong Leng	Northeast NT	639
10. Fei Ngo Shan (Kowloon Peak)	South Central NT	602
11. Tsing Shan (Castle Peak)	West NT	583
12. Pak Shek Kiu	Central NT	578
13. Tai Lo Shan (Tate's Cairn)	South Central NT	577
14. Pok To Yan	Lantau Island	576
15. Shui Ngau Shan (Buffalo Hill)	East NT	575
16. Kai Kung Leng	Northwest NT	572
17. Tai To Yan	North NT	565
18. Victoria Peak	Hong Kong Island	554
19. Kwun Yam Shan	Central NT	548
20. Pak Ka Shan (Mount Parker)	Hong Kong Island	531

Table 2 below summarizes the topography of Hong Kong in the form of hypsometric tables for elevations above 400 m PD calculated by Hill from Hong Kong Topographic Maps. The figures show the areas in square kilometres above each of the cited elevations. From this data it is clear that only a relatively small area, around 56 km^2, or just under 20 percent of the total land area of the HKSAR has an elevation exceeding 400 m PD.

Table 2. HKSAR Hypsometric Tables for Elevations over 400 m PD (*compiled by* Hill *from HK 1:50000 Topographic Maps, 1988*)

Location	>400m	>500m	>600 m	>700m	>800m	>900m
Tai Mo Shan	8.175	4.575	3.100	2.125	0.600	0.150
Ngong Ping & Lantau Peak	4.625	2.175	0.975	0.475	0.225	
Tai Tung Shan (Sunset Peak)	2.950	2.125	1.700	0.675	0.175	
Ma On Shan	1.375	0.725	0.175			
Tso Shan (Grassy Hill)	2.100	0.875	0.050			
Lai Pek Shan	3.250	1.000	0.025			
Tai Lo Shan (Tate's Cairn)	1.750	0.625				
Shui Ngau Shan (Buffalo Hill)	1.200	0.400				
Tai To Yan	1.525	0.125				
Pak Ka Shan (Mount Parker)	0.475	0.100				
Victoria Peak	0.450	0.050				
All Other Areas	28.325	0.325				
Total	56.200	13.100	6.025	3.275	1.000	0.150

iii) VEGETATION

In terms of vegetation, the ecological succession on the hillslopes of Hong Kong according to Ashworth *et al.* (1993) is from grassland to grassland with low shrubs, then tall shrubland and finally secondary forest. In the absence of disturbance, including fire, and on sites with suitable soil depths this may take 30 to 40 years. Based upon information presented in Ashworth *et al.* (1993) many of the upland areas in Hong Kong are covered in grass, grass and shrubs or shrubland. Shrubland may form the climax community on hillslopes where exposure prevents the growth of trees (Catt, 1986). Catt (1986) also reports that hill grasslands can be climax communities . She notes that the best-developed climax hill grasslands are found on the upper slopes of Tai Mo Shan, Ma On Shan and on the hillslopes of Lantau and Lamma Islands. She suggests that at these locations wind exposure, poor soil conditions and rapid runoff are limiting factors. Fire may also play an important role given the fire-prone nature of the Tai-Mo-Shan Country Park. For example, Dudgeon and Corlett (1994) suggest that the greater incidence of woodland on north facing slopes may reflect a micro-climate control on the incidence of fire. Many of the wooded areas in the uplands are plantation or afforested areas. In part this has been carried out to protect water gathering grounds which are extensive in the uplands. Good examples are provided by the hills around Tai Lam reservoir and the Kowloon reservoirs. However, Dudgeon and Corlett (1994) report that at high altitude (over 500 m PD) on Tai Mo Shan, Ma On Shan and on Sunset and Lantau Peaks there are patches of what may be primary woodland. They indicate that all are in areas which preclude fire *e.g* damp valleys or among boulders.

Figure 5. **Map of the Experimental Site on Tai Mo Shan**

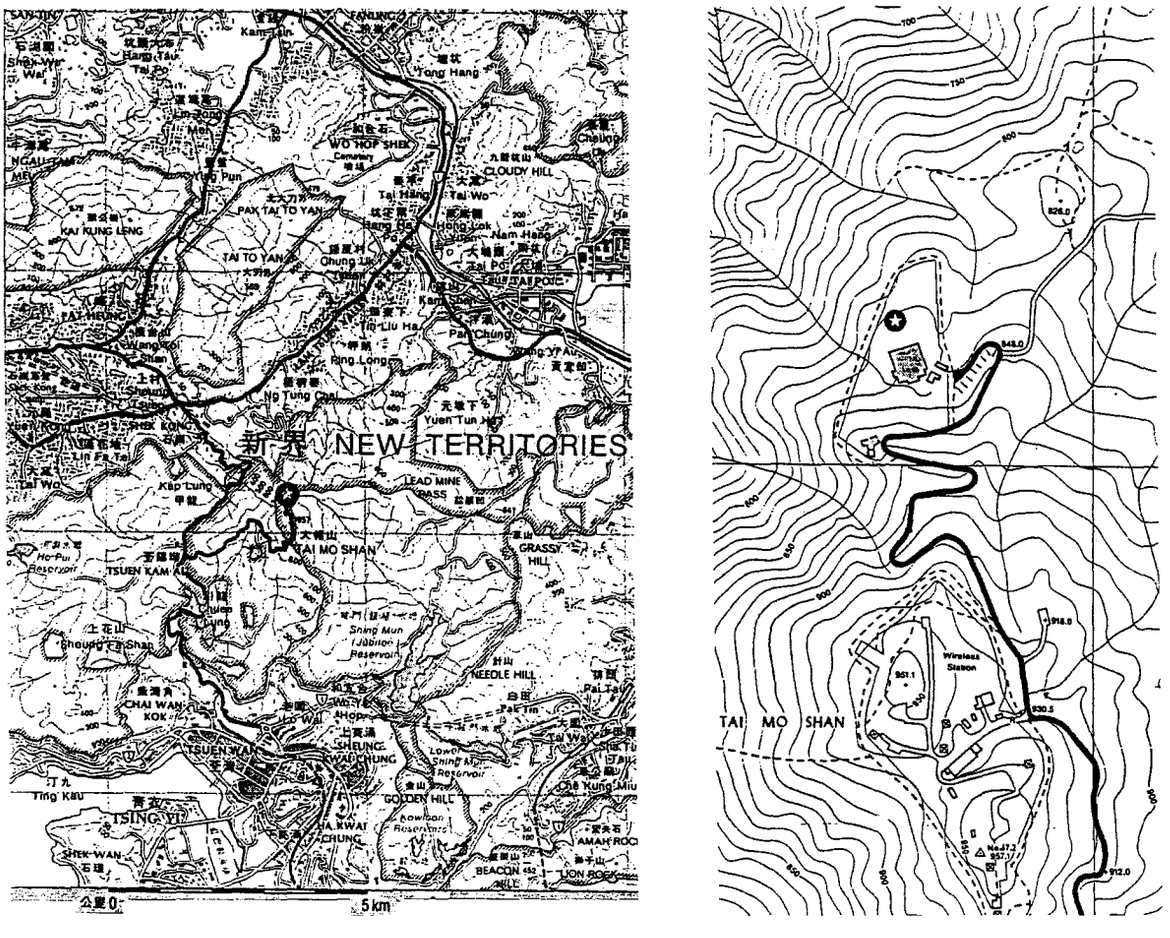

iv) THE SITE

At 957 m PD Tai Mo Shan is the highest point of Hong Kong. The actual peak is not accessible. However, due north of the peaks at around 825 m PD there was a secure compound which contained, amongst other things, an out-station site of the Observatory (Figure 5). Permission was granted to install a device to collect water from clouds. The site was selected because the high altitude maximised the number of days with low cloud or mist and fog. It was secure, and access was available by road. No obstruction existed near the site to intercept cloud, the vegetation being very short grass. Manpower was also available to take readings and monitor the physical well-being of the equipment.

Instrument Design and Construction

Due to the interest in cloudwater and interception on mountain slopes a variety of designs has been developed. In terms of ground based collectors Waldman *et al.* (1992) distinguishes between active and passive collectors. Where there is a power supply water can be extracted by means of a rotating arm, linear jet or fan-drawn collectors and these are reviewed by Waldman *et al.* (1992). Where no power is available to employ active collectors Waldman *et al.* (1992) state that passive ground based collectors are employed. He reports that: "Virtually all use some kind of plastic strings or screen mounted vertically in the wind. Droplets impact on the strings as they are advected past, and flow by gravity to a collection reservoir at the bottom". Such a device, termed a neblinometro, has been employed in this study and is described below.

The design of the neblinometro owes a great deal to the work carried out in Chile cited earlier. The basic design employed in that investigation was used as a basis for the design of the instrument built for Tai Mo Shan. This instrument consists of two subsystems, a collection subsystem and a measurement subsystem.

Figure 6. **Engineering Drawing of the Neblinometro**

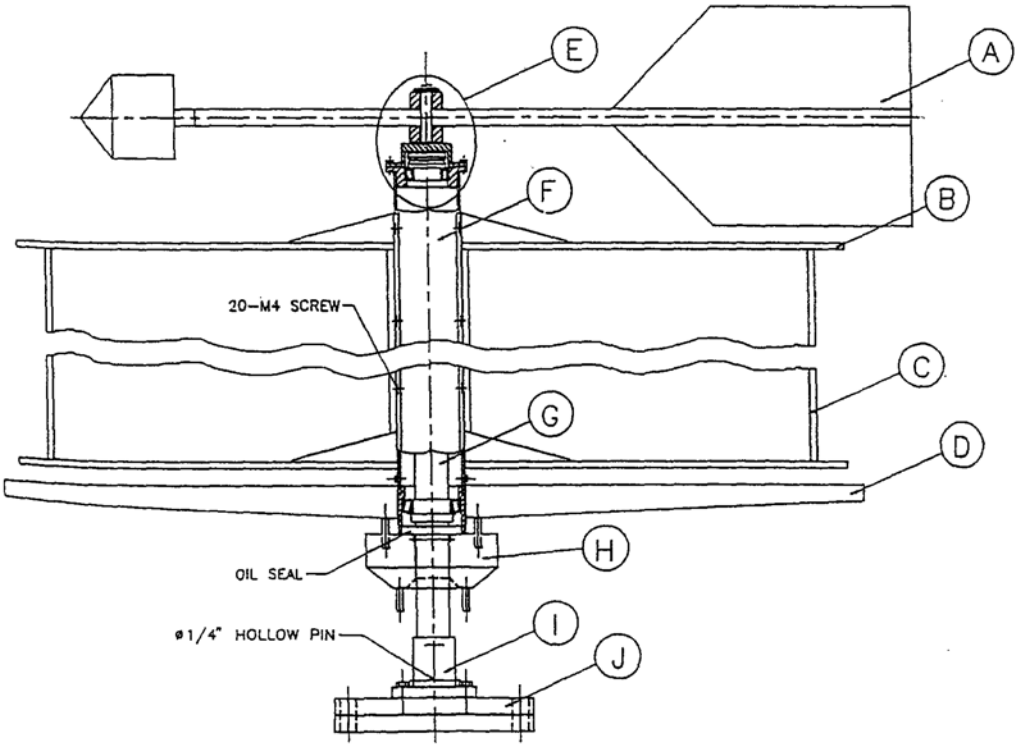

The engineering drawing ultimately produced in consultation with The University of Hong Kong Engineering Workshops for the collection subsystem is shown in Figure 6. The device is designed to capture the wind-blown cloud droplets on vertically aligned nylon filaments that are mounted in two separate panels (C) on a metal frame (B). Each panel size is 0.5 m by 0.5 m with a warp of 166 nylon threads of 0.4 mm diameter and a warp spacing of 0.3 mm. The total collection area was thus 0.25 square metres of which 103,750 square millimetres or about 20 percent was filament. The panels were designed to be removable to enable future experimentation with panels with different warp densities and to permit replacement in the event of damage.

The metal frame is fixed to a central sleeve (F) mounted on low-friction bearings to enable it to swivel through 360 degrees on a vertical post (G). Also attached to this sleeve directly below the metal frame is a shallow trough (D) which collects any cloud droplets intercepted by the panels, feeding them by gravity to a central reservoir (H) fixed to the vertical post (G). From this reservoir collected water is channelled via plastic tubing to the measurement subsystem.

A vane system (A) is attached perpendicularly to the axis of the metal frame at the top of the central sleeve (F). This ensures that the collection panels are always aligned orthogonally to the wind direction so permitting maximum surface area for interception as the cloud blows through the warp. The whole unit is bolted firmly at J to a vertically mounted I beam embedded in concrete for stability.

Figure 7. **Photograph of the Neblinometro Collection Subsystem**

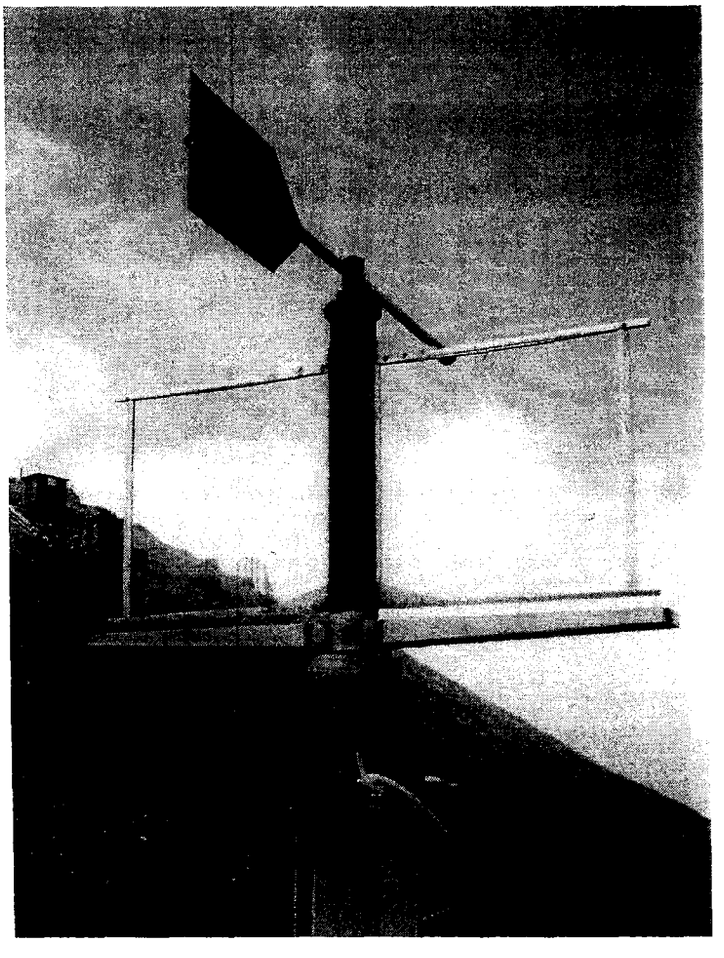

The measurements subsystem is based on a tipping-bucket mechanism similar to that found in rain gauges. After passing through a small still well reservoir designed to reduce inflow surges, the collected water from the panels is directed on a tipping-bucket. When either side of the bucket is full, the bucket tips drawing a magnet across a reed switch mounted on the unit, activating it and sending a pulse to the counter unit. The water so tipped is drained from the system to the ground. The counter unit itself is a simple battery powered unit that counts each pulse as the reed switch is activated. The counter uiit initially used an LCD display unit that counts each pulse as the reed switch is activated. However, this unit proved to be unreliable under field conditions and was replaced by an electromechanical counter supplied by an 8 volt battery. The number of counts from the unit in any measurement period is directly related to the number of tips of the bucket and hence the amount of water collected in that period.

The tipping-bucket can be calibrated either to a specific volume of water per tip or to an equivalent amount of rainfall received by a standard gauge per tip. The latter choice was made in order to enable estimates of the cloud water collected to be made in terms of equivalent precipitation. For an 8" standard gauge this equates to an average tip of 16.21 cc for each 0.5 mm of rainfall. Thus the number of counts in any period can either be multiplied by 0.0162 to obtain the cloud water yield in litres or by 0.5 to obtain the equivalent amount of precipitation in mm.

Preliminary Results

The neblinometro was exposed at a site on the north face of Tai Mo Shan at an elevation of about 830 m PD (Figure 5). The instrument was first exposed and readings began in April 1991. Figure 8 shows a photograph of the neblinometro in operation at the Tai Mo Shan site.

Figure 8. **Photograph of the Neblinometro on Site at Tai mo Shan**

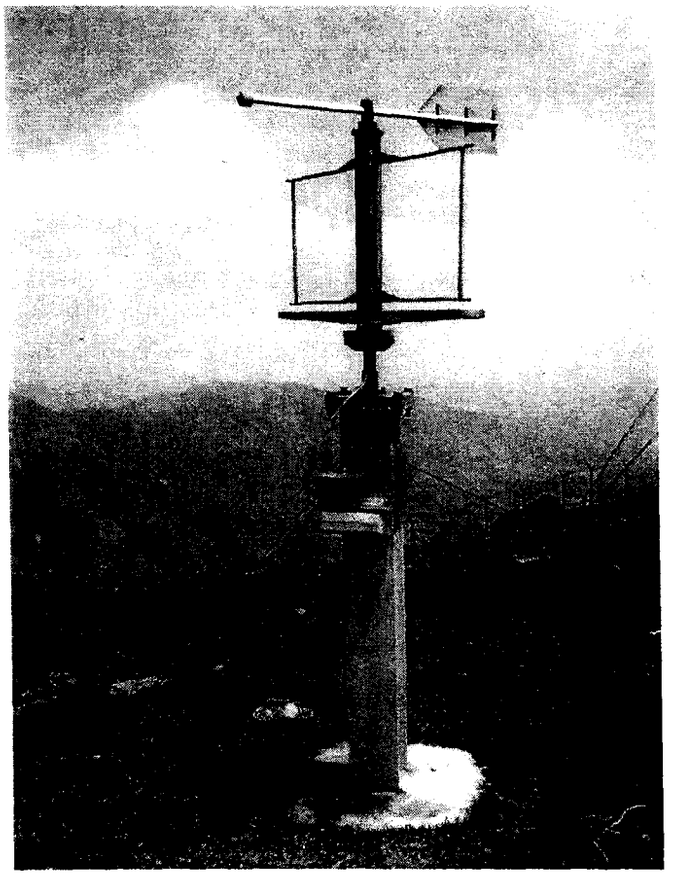

Waldman *et al.* (1992) observe that : "A major problem with these devices is that collection rates depend on wind speed, in calm or low wind, no sample will be collected. In addition, collection efficiencies vary greatly with the ambient wind velocity. Depending on the diameter of the strings, high winds may be required for collection of representative samples. With 0.5 mm diameter strings, wind speeds over 5 ms^{-1} are required to collect efficiently droplets larger than 5μm." It is our experience, however, that high winds will remove some droplets from the vertical collector strings before they have time to reach the collecting tray. Moreover, at Tai Mo Shan light winds are the exception rather than the rule. The neblinometro, as modified, proved to be sturdy and reliable though exposed to winds in excess of 27 m s^{-1}.

Readings were taken by observers twice a day, at 0900 and 1500, concurrent with the regular observation schedule. As well as recording the counter reading, the observers were asked to note the rainfall reading and the current weather condition. The former enabled separation of the data into two sets, those collected in the absence of precipitation and those when precipitation occurred during the measurement period. The latter was intended primarily to ascertain whether, during dry periods, there was cloud cover on the site and its nature and density.

Despite a number of initial observational problems, mainly associated with the electronics of the measurement subsystem, a fairly comprehensive record has been accumulated over a nearly 2 year period which enables some preliminary results to be presented.

The first finding that can be stated categorically is that the instrument works! That is, it is capable of extracting water from the cloud passing through the collection screens. In some circumstances this can be a considerable amount of water. The largest amount collected, during a 24 hour period when no rain was recorded at the site, amounted to 17.7 litres from 0900 on 5 February to 0900 on 6 February 1992.

Secondly, considerable amounts of cloud moisture were extracted during the spring months of February, March and April with amounts ranging from a minimum of about 1.5 litres per day when clouds were present at the site. By contrast during other months of the year the yield, in non-rain periods, was very substantially reduced, ranging between 0.1 and 0.5 litres per day even when the site was covered in cloud for most of the time.

This marked contrast suggests that for the configuration at present being used for the collection screens the droplet size distribution and air flow patterns associated with spring-time stratus cloud are more conductive to higher collection efficiencies. At this time of year, moist easterly and northeasterly air masses moving off the south China Sea form stratiform clouds beneath the elevated inversion of the winter monsoon. Such flows are channelled up the north face of Tai Mo Shan to the collector.

In summer, however, the predominant flow direction is from the south. During dry periods, convection activity is strong and cloud cover at the site level is not common. When it does occur, the droplet size would seem to be much smaller than in the spring so precluding much extraction of cloud moisture from such clouds by the existing equipment.

Acknowledgements

Financial support for the investigation was provided by the Woo Ting Sang Agricultural Development Research Fund of The University of Hong Kong, which is gratefully acknowledged. Records at Tai Mo Shan were maintained by police staff of the Composite Signal Organization Station under the direction of successive officers-in-charge, Messrs. Bentley, Mayes, Cork and Wilson. To all of them our grateful thanks.

References

Ashworth, J.M., Corlett, R.T., Dudgeon, D., Melville, D.S. and Tang, W.S. (1993) *Hong Kong Flora and Fauna: Computing Conservation.* World Wide Fund for Nature, Hong Kong.

Baker, E.T. and Hughes, R.G. (1956) *An analysis of low cloud and poor visibility at Sek Kong, May 1951 to April 1955*,. Royal Observatory Technical Note No. 16, Royal Observatory, Hong Kong.

Catt, P. (1986) Vegetation. *in* T.N. Chiu and C.L. So (eds)., *A Geography of Hong Kong (2nd Ed.)*, Oxford Univ. Press, Hong Kong, 118-147.

Cannon, W.A. (1901) On the relation of redwoods and fog to the general precipitation in the Redwood Belt of California. *Torreya*, **1**, 137-139.

Cavelier, J. and Meija, C.A. (1990) Climatic factors and tree stature in the elfin cloud forest of Serrania de Macuira, Colombia. *Agric Forest Meteor.*, **53**, 105-123.

Cereceda. P., Schemenauer, R.S. and Suit, M. (1992) An alternative water supply for Chilean coastal desert villages. *Water Resources Development*, **8**(1), 53-59.

Chandler, A.S., Choularton, T.W., Dollard, G.J., Gay, M.J., Hill, T.A., Jones, A., Jones, B.M.R., Morse, A.P., Penkett, S.A. and Tyler, B.J. (1988) A field study of the cloud chemistry and cloud microphysics at Great Dun Fell. *Atmospheric Environment*, **22**(4), 683-694.

Chin, P.C. (1986) Climate and weather. *in* T.N. Chiu and C.L. So (eds.), *A Geography of Hong Kong. (2nd Ed.)*, Oxford Univ. Press, Hong Kong, 69-85.

Cheng, S.S.M. (1987) *Dry spells during mid-summer over south China.* Royal Observatory Technical Note No. 44, Royal Observatory, Hong Kong.

Cooper, W.S. (1917) Redwood, rainfall and fog. *Plant World*, 20, 179-189.

Dudgeon, D. and Corlett, R. (1994) *Hills and Streams: an ecology of Hong Kong.* Hong Kong University Press, Hong Kong.

Ekern, P.C. (1964) Direct interception of cloud water at Lanaihale, Hawaii. *Proc. Soil Sci. Soc. America*, **28**(3), 419-421.

Falconer, R.E. and Falconer, R.D. (1980) Determination of cloud water acidity at a mountain observatory in the Adirondack Mountains of New York State. *J. Geophys. Res.*, **85**, 7465-7470.

Fletcher, C.J.N., S.D.G. Campbell, J.P. Busby, R.M. Carruthers, and K.W. Lai (1997) Regional tectonic setting of Hong Kong: implications of new gravity models. *J. Geol. Sci.*, **154**, 1021-1030.

Gindel, I. (1966) Attraction of atmospheric moisture by woody xerophytes in arid climates. *Commonwealth Forest Rev.*, **45**, 297-321.

Glas, G. (1764) History of the Canary Islands. *Quoted in* (1960) *Weather*, **15**, 374.

Gurnell, A.M. (1976) A note on the contribution of fog drip to stream flow. *Weather*, **31**, 121-126.

Huang, Bing-Wei (1959) A scheme for comprehensive physical regionalization of China. *Sci. Bull.*, **9**, (in Chinese), *cited in* Zhao Songqiao (1986) *Physical Geography of China* , Science Press, Beijing, 95.

Hutley, G.B., Doley, D., Yates, D.J. and Boonsaner, A. (1997) Water balance of an Australian subtropical rainforest at altitude 1. The ecological and physiological significance of intercepted cloud and fog. *Austral. J. Bot.*, **45**, 311-329.

Jackson, I. and Hsu, S.I. (1992) *Aspects of rainfall and water balance of Hong Kong.* Occasional Paper, Department of Geography, The Chinese University of Hong Kong.

Juvik, J.O. and Perreira, D.J. (1974) Fog interception on Maura Loa, Hawaii. *Proc. Assoc. Amer. Geographers*, **8**, 22-25.

Kerfoot, O. (1968) Mist precipitation on vegetation. *Forestry Abstracts*, **29**, 8-20.

Lovett, G.M., Reiners, W.A. and Olsen, R.K. (1982) Cloud droplet deposition in subalpine balsam fir forests: hydrological and chemical inputs. *Science*, **218**, 1303-1304.

Phillips, J.F.V. (1976) Rainfall interception by plants. *Nature*, **118**, 837-8, 915.

Schemenauer, R.S. (1988) Fog water to quench a desert's thirst. *WMO Bulletin*, **37**, 281-286.

Schemenauer, R.S., Fuenzalida, H. and Cereceda, P. (1988) A neglected water resource: the Camanchaca of South America. *Bull. Amer. Meteor. Soc.*, **69**(2), 138-147.

Schemenauer, R.S. and Cereceda, P. (1991) Fog water collection in arid coastal locations. *Ambio*, **20**(7), 303-308.

Schemenauer, R.S. and Cereceda, P. (1992) The quality of fog water collected for domestic and agricultural use in Chile. *J. App. Meteor.*, **31**(3), 275-290.

Stadtmuller, T. (1987) *Cloud forests in the humid tropics: a bibliographic review.* The United Nations University, Costa Rica.

Starbuck, L. (1950) *A statistical survey of Hong Kong rainfall.* Royal Observatory Technical Memoir No. 2, Royal Observatory, Hong Kong.

Styles, K.A. and Hansen, A. (1989) *Territory of Hong Kong, Geotechnical Area Studies Programme. GASP Report XII.* Geotechnical Control Office, Civil Engineering Services Dept., Hong Kong Government, Hong Kong.

Waldman, J.M., Munger, J.W. and Jacob, D.J. (1992) Measurement methods for atmospheric acidity and acid deposition. *in* M. Radojevic and R.M. Harrison (eds.) *Atmospheric Acidity, Sources, Consequences and Abatement.* Elsevier, London and New York, 205-243.

White, G. (1789) *Natural history and antiquities of Selbourne.* Aldine Edition (1898) McMillan, London.

HONG KONG METEOROLOGICAL SOCIETY

INFORMATION FOR CONTRIBUTORS TO THE BULLETIN

Technical or research articles, as well as reviews and correspondence of a topical nature are welcome. In general contributions should be short, although exceptions may be made by prior arrangement and at the sole discretion of the Editorial Board. Copyright of material submitted for publication remains that of the author(s). However, any previous, current, or anticipated future use of such material by the author must be stated at the time of submission. All existing copyright materials to be published must be cleared by the contributor(s) prior to submission.

Manuscripts must be accurate and preferably in the form of a diskette containing an electronic version in one of the common word processing formats. WORD is preferred but others are also acceptable. Whether or not an electronic version is submitted, two complete manuscript copies of the articles should be submitted. These should be preceded by a cover page stating the title of the article, the full name(s) of the author(s), identification data for each author (position and institution or other affiliation and complete mailing address). An abstract of about 150 words should be included. Manuscripts should be double-spaced, including references, single-side only on A4 size paper with a 2.5 cm margin on all sides, and be numbered serially. All references should be arranged in alphabetical and, for the same author, chronological order. In the text they should be placed in brackets as (Author'(s) name(s), date). In the reference list at the end the Author'(s) name(s) and initials followed by the date and title of the work. If the work is a book this should be followed by the publisher's name, place of publication and number of pages; or, if a journal article, by the title of the periodical, volume and page numbers.

Submission of electronic versions of illustrations is encourage. Originals of any hardcopy illustrations submitted should be in black on tracing material or smooth white paper, with a line weight suitable for any intended reduction from the original submitted size. Monochrome photographs should be clear with good contrasts. Colour photographs are also accepted by prior arrangement with the Editorial Board. Originals of all illustrations should be numbered consecutively and should be clearly identified with the author'(s) name(s) on the back. A complete list of captions printed on a separate sheet of paper.

All submitted material is accepted for publication subject to peer review. The principal author will be sent comments from reviewers for response, if necessary, prior to final acceptance of the paper for publication. After acceptance the principal author will, in due course, be sent proofs for checking prior to publication. Only corrections and minor amendments will be accepted at this stage. The Society is unable to provide authors with free offprints of items published in the Bulletin, but may be able to obtain quotations from the printer on behalf of authors who express, at the time of submission of proofs, a desire to purchase a specified number of offprints.

Enquiries and all correspondence should be addressed to the Editor-in-Chief, Hong Kong Meteorological Society Bulletin, c/o Department of Geography, The University of Hong Kong, Pokfulam Road, Hong Kong. (*Tel. +(852) 2859-7022; Fax. +(852) 2559-8994 or 2549-9763; email: billkyle@hkusua.hku.hk or billkyle@hkucc.hku.hk.*

香港氣象學會

HONG KONG METEOROLOGICAL SOCIETY

Bulletin

Volume 10, Numbers 1/2, 2000

SINGLE COPY PRICE: HK$ 150

(for subscription rates see inside front cover)

CONTENTS